TITLE PAGE

Report Title: Feasibility of Large-Scale Ocean CO_2 Sequestration

Type of Report: Technical Progress Report

Reporting Period Start Date: October 01, 2001

Reporting Period End Date: September 30, 2002

Principal Authors: Dr. Peter Brewer, Dr. James Barry

Date Report was Issued: September 2002

DOE Award Number: DE-FC26-00NT40929

Name and Address of Submitting Organization:

Monterey Bay Aquarium Research Institute
7700 Sandholdt Road
Moss Landing, CA 95039-9644

Washington University at St. Louis **(Subcontract)**
Dept of Earth and Planetary Sciences
Campus Box 1169
One Brookings Drive
St. Louis, MO 631031

Abstract

We have continued to carry out creative small-scale experiments in the deep ocean to investigate the science underlying questions of possible future large-scale deep-ocean CO_2 sequestration as a means of ameliorating greenhouse gas growth rates in the atmosphere. This project is closely linked to additional research funded by the DoE Office of Science, and to support from the Monterey Bay Aquarium Research Institute. The listing of project achievements here over the past year reflects these combined resources.

Within the last project year we have:

1. Published a significant workshop report (58 pages) entitled "Direct Ocean Sequestration Expert's Workshop", based upon a meeting held at MBARI in 2001. The report is available both in hard copy, and on the NETL web site.
2. Carried out three major, deep ocean, (3600m) cruises to examine the physical chemistry, and biological consequences, of several liter quantities released on the ocean floor.
3. Carried out two successful short cruises in collaboration with Dr. Izuo Aya and colleagues (NMRI, Osaka, Japan) to examine the fate of cold (-55ºC) CO_2 released at relatively shallow ocean depth.
4. Carried out two short cruises in collaboration with Dr. Costas Tsouris, ORNL, to field test an injection nozzle designed to transform liquid CO_2 into a hydrate slurry at ~1000m depth.
5. In collaboration with Prof. Jill Pasteris (Washington University) we have successfully accomplished the first field test of a deep ocean laser Raman spectrometer for probing *in situ* the physical chemistry of the CO_2 system.
6. Submitted the first major paper on biological impacts as determined from our field studies.
7. Submitted a paper on our measurements of the fate of a rising stream of liquid CO_2 droplets to Environmental Science & Technology.
8. Have had accepted for publication in Eos the first brief account of the laser Raman spectrometer success.
9. Have had two papers submitted for the Greenhouse Gas Technology – 6 Conference (Kyoto) accepted.
10. Been nominated by the U.S. Dept. of State to attend the Nov. 2002 IPCC Workshop on Carbon Capture and Storage.
11. Given presentations at national meetings, including the AGU Ocean Sciences Meeting, the American Chemical Society, the Minerals, Materials, and Metals Society, the National Academy of Engineering, and given numerous invited lectures..

Copies of relevant documents, including the report from Prof. Pasteris, and several papers, are attached here.

TABLE OF CONTENTS

LISTS OF GRAPHICAL MATERIALS

Results of Ocean Chemical and Biological Studies

Results of the Direct Ocean CO_2 Sequestration Workshop.

The results of this 2001 workshop, attended by scientists of 7 nations, are available on line at MBARI and NETL as well as in hard copy. A recommended time line and priorities for research was arrived at, and essential research strategies discussed. The results have influenced program development, and encouraged scientists who had not previously contributed to this field to become engaged. The report itself is too big to be appended to this document and is separately available.

Release of Cold (-55ºC) CO_2 at Intermediate Ocean Depths.

We have carried out two cruises in early 2002 in collaboration with Dr. Izuo Aya and colleagues to investigate the behavior of tanker transported liquid CO_2 injected into the ocean. The cold CO_2 is more dense than sea water, and thus may potentially be capable of sinking rapidly below the injection point, thus avoiding the cost of deep injection by pipeline. However fluid dynamic instabilities can also lead to liquid break up into small units, and rapid thermal equilibrium. We observed initial rapid sinking, a brief neutral buoyancy point, and then slow rise of the mass. Analysis of the trajectories revealed ways to minimize these effects, and to maximize the sinking depth achieved. (See attached paper). This involves creating a slurry of dry ice within the liquid phase, thus changing the density and heat capacity. The sinking rate, and depth of dissolution, are thus under operational control. This may lead to minimal environmental effects due to a more widespread dissolution zone, and lower cost and increased safety procedures, from the far shorter pipes required.

Deep Ocean Experiments

We have carried out a series of three cruises in April 2002 to investigate the fate and biological consequences of liquid CO_2 disposed of on the sea floor at 3600m depth. Our 56L capacity CO_2 delivery system worked well, and 4 controlled delivery dives were executed with the CO_2 delivered to a central corral complex. An image (below) taken during the experiments shows the three corral units, with trapped and caged marine animals (fish, octopus, amphipods) placed close by. A time lapse camera, a current meter, and a set of recording CTD-pH sensors, completed the experimental complex. A full account of results obtained to date has been prepared in manuscript form (Barry et al., 2002), and this is appended here.

The results showed a strong tidal periodicity in the plume of lowered pH water, and a complex set of biological responses.

Image of the central corral complex and associated equipment at 3600m depth. The three white corrals are partially full of CO_2. The cage to the right contains an octopus, several fish, and an amphipod cage, all in very close proximity to the CO_2 source. A time lapse camera is partially visible at top right, and a recording CTD-pH sensor at top center.

Progress Report from Washington University

Year 2 Summary of Projects Completed in Conjunction with DoE Collaboration with MBARI during the Period of 1 July, 2001 through 1 July, 2002

Submitted by Jill Pasteris, John J. Freeman, Brigitte Wopenka

Our interactions with and laboratory experiments on behalf of MBARI involved five different types of tasks this past year: 1) development of standards and protocols to calibrate Raman spectra acquired on the sea floor, 2) studies to optimize the collection of a Raman signal from samples of interest on the sea floor, 3) enlargement of the Raman database of minerals, 4) testing the applicability of Raman spectroscopy to sediments removed from the sea floor, and 5) aiding MBARI personnel in Raman spectroscopic analysis through spectral interpretation and technical training.

The following report is written so that the **bolded headings** and the *italicized sentences* that follow them can be read as an executive summary. More detailed statements follow beneath each heading.

1. Development of Raman Spectroscopic Standards for Calibration of the Deep-Sea Raman System.

For pre-dive calibration of wavelength, we recommend argon and/or neon gas-emission lamps, cyclohexane, diamond, silicon, and the mineral hydroxyl-apophyllite. For sea-floor calibration, we recommend diamond, hydroxyl-apophyllite, and a plastic (still under investigation).

Before the spectrometer is deployed on the sea floor (while in its pressure housing and, preferably, still in the lab), we recommend use of a wavelength-calibration (gas-emission; either Ne or Ar or both) lamp to establish the mapping of wavelengths to pixels; a white-light intensity standard to establish proper relative intensities across the entire, recorded spectral region; and a Raman-shift standard such as cyclohexane to determine the exact laser wavelength. The combination of the wavelength calibration for the spectrometer and the wavelength calibration for the laser establishes the desired wavenumber shift (Raman peak-position) calibration for the entire laser-spectrometer-detector system.

Our lab tests showed that cooling of diamond and of isopropanol from 24☜C to 2☜C produced an upshift of about 0.3-0.5 cm^{-1} in the recorded Raman band positions. Temperature change to the sample alone, however, is only one of the factors that affect the signal intensities and peak positions recorded in a Raman spectrum on the sea floor. When the spectrometer itself is deployed underwater, additional calibration is needed to account for the effects on the spectrometer of temperature changes and pressure-induced deformation of the pressure housing and optical cables. We recommend the use of both a standard that is permanently mounted within the Raman probe head (small diamond wafer) and a portable standard that can be analyzed as desired and that has numerous sharp bands in both the low- and high-wavenumber regions (the mineral apophyllite or a suitable plastic). Such calibration will make it possible to record Raman peak positions with accuracies within ± 1 cm^{-1}. Precision in the measurement of Raman peak positions in the lab is shown to be about ± 0.2 cm^{-1} and on the ocean floor about ± 0.4 cm^{-1}.

2. Optimizing Collection of a Raman Signal from Samples on the Sea Floor

Several analytical objectives are listed in the DoE proposal. This past year, the focus of study has been on interfaces, i.e., liquid-liquid, solid-solid, and solid-liquid interfaces on the ocean floor. The goal is to measure chemical-structural properties at the interface and at defined distances from the interface. This goal involves a) optimizing the optical elements of the instrument for delivery of the laser and capture of the Raman signal and b) coping with the sampling geometry and physical-optical properties of the sample of interest, e.g., clathrate hydrate.

a. Evaluation of Depth of Field and Focal Length of Underwater Optical Lenses: Efficiency of Signal Capture and Rejection of Extraneous Signal during Analysis. *It is a demanding analytical challenge to make Raman measurements at an interface while the sampling optics are underwater. Selection of a lens with a large depth of field makes it difficult to analyze the properties exclusively at the interface, whereas a short depth of field makes it very difficult to focus on an object/interface by means of a coarse mechanical manipulator (e.g., ROV arm). Additional problems arise from the capture of Raman signals "extraneous" to the desired sample, i.e., signal that arises from the medium (e.g., sea water) between the objective and the sample. For analysis of interfaces and samples on each side of an interface, an objective with a shorter focal length (i.e., stand-off distance) will be needed in order to reduce signal from the intervening seawater. We are investigating which individual lenses will best suit specific types of analyses required on the sea floor.*

Each objective lens has a specific depth of field. We tested in detail the stand-off optic with a 2.5-inch focal length (identical to the one deployed by MBARI on the sea floor) in our hand-held probe head. The signal intensity was recorded as a function of the objective's distance from an opaque solid sample. The depth of focus is about 1 mm (defined as the distance over which the monitored Raman signal is ≃50% of the maximum value). MBARI personnel has determined that the 2.5-inch focal length in air is increased to 8 inches underwater. Direct extrapolation of that elongation factor indicates that the stand-off optic will have a depth of field of about 3.2 mm underwater. The length of the depth of field imposes the level of accuracy required for positioning of the Raman probe head by the ROV's manipulator arm.

Objective lenses with long focal lengths have been used in the first iteration of the underwater Raman system to accommodate the lack of fine control on the positioning of the head. Such objectives have the disadvantages of inducing Raman scattering (and capturing its signal) from sea water in the intervening optical path and typically having large depths of field (lack of specificity of target volume). We now are investigating various immersion probe optics to minimize the depth of field (to produce a "tight" beam spot on the sample of interest) and the Raman scattering from the background medium. Note the latter entails the need for a fine-control motorized stage to accurately position the probe head.

b. Evaluation of Scattering Losses from Surfaces. *Scattering losses at surfaces (i.e., interfaces) will decrease the intensity of the incident laser on the material of interest, prevent the laser from penetrating deeply into the sample, and decrease the intensity of the Raman signal that reaches the detector. We are investigating ways to cope (through selection of optical elements and sampling geometry) with fine-grained polygranular aggregates such as the CO_2 clathrate hydrates formed synthetically on the sea floor. The goal is to acquire good Raman spectra of clathrate hydrate in the presence of liquid CO_2 and seawater on the ocean floor.*

We need to learn how to minimize and to cope with light scattering from surfaces – a phenomenon that degrades the intensity of the Raman signal from a sample. For analyses on the ocean floor, two types of signal-loss due to scattering should be considered: those due to rough or

"hazy" (e.g., polygranular, inclusion-rich) surfaces and those due to large differences in refractive index between water (n=1.34) and the object of interest. Directing the laser perpendicular to a smooth interface will minimize light loss due to differences in refractive index. For the analysis of optically hazy, polygranular samples, such as clathrate hydrate, we continue to explore the use of different optical lenses and sampling geometries.

We have investigated the intensity losses of Raman scattering as exhibited in compact powders and rough, solid surfaces. Measurement of the signal intensity from such samples shows that specular reflection losses can be minimized by decreasing the difference in refractive index between the sample and the surrounding medium, i.e., by changing from analysis in air ($\eta = 1.00$) to analysis in water ($\eta = 1.34$), using the microprobe configuration of our instrument and a water-immersion objective. Raman scattering from a roughly sawn mineral surface immersed in water is as strong as the Raman scattering from a highly polished surface of the same sample in air. This comparison demonstrates that Raman spectroscopy underwater has the advantage of decreasing the amount of light scattering at interfaces, especially from polygranular samples, but that such analysis also introduces extraneous signal from the intervening water medium, as discussed above.

3. Enlargement of Raman Database of Minerals.

Relatively well characterized mineral standards were analyzed in the "silica", feldspar, mica, and zeolite groups. The spectra were evaluated, and the best representatives were added to our Grams 32 Spectral ID searchable database, which we will make available to MBARI.

4. Ex-situ Raman Spectroscopy of Minerals in Deep Ocean Mud.

We determined the optimal Raman sampling conditions for recording, ex-situ, the Raman spectra of mineral particles in mud samples taken from the ocean floor in Monterey Bay. Spectra can be recorded effectively on the mineral particles only with the microprobe configuration. Indeed, we found that the stand-off optic will be of almost no use in taking mineral spectra in situ on the sea floor due to the inherent high fluorescence of the organic component of the mud and the inability of the stand-off optic to excite Raman scattering sufficiently to bring its signal above that of the fluorescence.

We developed analytical protocols for recording the Raman spectra from mineral particles while minimizing interference from laser-stimulated fluorescence of the organic material that occurs together with the minerals. The best data are acquired with a Raman system in the *microprobe* configuration using 50X to 150X magnification microscope objectives (water-immersion or standard air-medium type) to collect the Raman data. This configuration permitted the isolation and recording of Raman spectra from single mineral particles in the mud matrix while minimizing fluorescence interference.

This technique was used in a Raman survey of the distribution of minerals in a set of mud samples retrieved from the ocean floor at or near sites of liquid CO_2 deposition. The mud at this site in Monterey Bay was shown to be dominated by well crystalline to poorly crystalline forms of silica; several types of feldspars, phyllosilicates , iron oxides, and titania polymorphs; sphene; and small amounts of apatite.

5. Spectral Interpretation and Technical Training.

a. Spectral Interpretation of Data from Dives T417, T418, T420 and T421. *The importance of wavelength and intensity calibration of the system on the sea floor was made clear.*

Post-dive modifications to the spectra made interpretation possible. We interpret the lack of success in obtaining spectra on an obvious chunk of clathrate hydrate as due, in large part, to: the overwhelming signal of the intervening ocean water (see #2a above) and light scattering by the polygranular clathrate hydrate (see #2b above), which diminished the laser's penetration into the sample.

One or more members of the group Pasteris, Freeman, and Wopenka participated in four of the recent successful deployments of the MBARI ocean Raman system on the sea floor at depths to 3600m. We participated in the writing of a short communication that was submitted to the journal *Science*.

b. Raman Spectroscopic Training for MBARI Personnel. *Dr. Edward T. Peltzer and Dr. Sheri White spent several days each in our Raman laboratory.*

Dr. Edward Peltzer of MBARI visited our laboratory for 5 days during which we familiarized him with the KOSI Raman spectrometer system including the instrument and computer operation, spectrometer calibration, and use of various sampling optics. Dr. Sheri White of MBARI visited our laboratory for 3 days during which we showed her more advanced computer applications in spectral acquisition and interpretation. She also participated in several Raman spectroscopic experiments to enhance the acquisition of Raman spectra during instrument operation on the sea floor.

We are continuing to work on issues of importance to the accuracy, signal:noise ratio, and interpretation of Raman spectra taken on the sea floor. These include, but are not limited to: optimization of the collection optic for enhanced analysis of interfaces and rejection of signal outside the focal volume, testing of Raman standards suitable for use on the deep ocean floor, and interpretation of Raman spectra already collected on the ocean floor (e.g., effect of pressure on the Raman spectrum of CO_2, as analyzed at known depths).

APPENDIX I
COPIES OF PAPERS SUBMITTED TO GHGT-6, KYOTO

Advances in Deep-Ocean CO_2 Sequestration Experiments

P.G. Brewer[1], E.T. Peltzer[1], G. Rehder[2] and R. Dunk[1]

[1] Monterey Bay Aquarium Research Institute
7700 Sandholdt Road, Moss Landing CA 95039, USA
[2] GEOMAR Center for Marine Research
Wischofstr. 1-3, Kiel, D-24148, Germany

Abstract

We report on advances made in carrying out small-scale experiments on the direct injection of CO_2 in the deep ocean using ROV technology [1]. We have developed a carbon-fiber composite accumulator of 56L internal capacity for safe CO_2 containment and delivery and have used this for a series of experiments at 3600m ocean depth, thus enabling delivery of sufficient CO_2 for biological response studies. We have also developed a time-lapse camera for recording events associated with the CO_2 pool. A newly developed laser Raman spectrometer has been used to obtain spectroscopic information *in situ*, thus enabling detection of the state of the CO_2, and the fate of impurities. We have measured a CO_2 dissolution rate of 1.7 $\mu mol/cm^2/sec$ by direct insertion of a pH probe into the liquid surface, thereby forming a pocket of water. This technique provides confirmation of the very rapid re-building of the hydrate skin reported by Aya et al. [2] in which surface cracks are quickly annealed. The presence of a hydrate skin exerts a strong effect on CO_2 chemical and physical properties, and we have observed quasi-chaotic instabilities associated with this phenomenon in which a transformation from thin film to massive hydrate formation has occurred within a few hours.

Introduction

Over the last five years we have developed and refined the techniques first described by Brewer et al. [1] for carrying out controlled releases of CO_2 on the ocean floor. The purpose of these experiments is to provide fundamental data on the chemical and physical behavior of the released material and, through a related program, to initiate biological response studies. In earlier work we have successfully carried out studies of small-scale releases of a rising stream of CO_2 droplets [3] at relatively shallow depth (800 – 400m), and have determined a dissolution rate of 3 $\mu mol/cm^2/sec$. Here we focus on studies at depths >3000m where the high compressibility of CO_2 relative to sea water leads to gravitational stability. Oceanic GCMs show that efficient retention of injected CO_2 is a strong function of depth [4] and thus there is great interest in deep injection properties.

Current Research

CO_2 Containment and Delivery

We have developed a 56L carbon-fiber composite piston accumulator (Hydratech, Fresno, CA), 23cm outside diameter, 194cm length, rated at 3000 psig, for ROV operation. Two tandem cylinder pumps, of 128ml and 970ml capacity, provide power for accurate delivery of the contained CO_2. Cooling, and compression, of the CO_2 during descent to ocean depth occurs so that under typical conditions (900 psig on deck at 16°C; 1.6°C at 3600m) 45.0L is available per dive for experimental purposes.

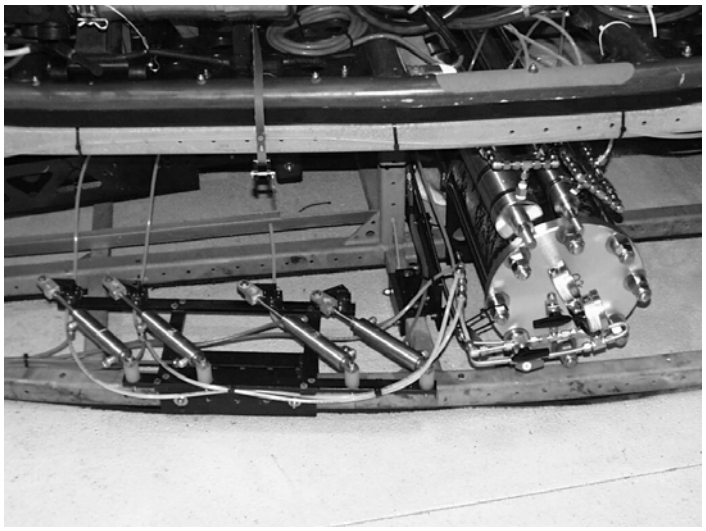

Figure 1: The 56L CO_2 delivery system installed on ROV Tiburon, showing end cap with gauges, delivery pumps on top, and valves to the left. The dispensing valve is attached to the robotic arm in front of the vehicle and is not shown.

Measurement of Dissolution Rates

Early ideas of oceanic CO_2 sequestration envisaged "permanent" disposal as a hydrate, however it was soon realized that the saturation condition was not met, and that hydrates would dissolve [5,6]. The saturated boundary layer model is the standard for understanding the dissolution rates of oceanic gases [7] and solids [8], and it may be applied to hydrate dissolution rates in the deep ocean [3, 9]. The solubility of CO_2 in contact with a hydrate phase changes only by a factor of ~2 from 800m to 3600m depth [5], and thus we may expect a dissolution rate about 50% of that determined from rising droplet studies [3] or about 1.5 μmol/cm^2/sec. We have confirmed this by depositing ~ 2L CO_2 on the sea floor, and inserting a pH electrode protected by a slotted metal cage (3cm diameter) directly into the surface (Figure 2). The CO_2 surface deforms not by elastic stretching, but by rapid re-building of the hydrate film [2]. A water pocket is thus formed in which the pH rapidly drops due to hydrate dissolution/CO_2 invasion. We observed a pH drop of 4.19 pH units in 15 minutes. Taking local alkalinity as 2442 μmol/kg, we calculate a CO_2 accumulation rate of 2913 μmol/kg/sec, and a dissolution rate of 1.7 μmol/cm_2/sec, in close agreement with the estimate above. The lowest pH observed corresponds to a solution of ~2 molar, about a factor of 3 greater than the equilibrium saturation value, and thus unstable with respect to very rapid hydrate formation upon nucleation.

Figure 2: Image of the pH probe inserted into a mass of CO_2 on the sea floor at 3600m depth. Hydrate film re-building allows formation of a water pocket ~3cm deep in which pH drops in response to CO_2 invasion of the aqueous phase.

Evidence for Quasi-chaotic Hydrate Dynamics

In our first experiment at depth [1] we used a laboratory beaker to contain CO_2 on the sea floor. We observed large volume changes, driven by hydrate dynamics, and a series of dramatic spillover events occurred; Aya et al. [10] have established the critical role of formation of a water channel to create the observed convective instabilities. In a later, near identical, field experiment we did not observe these instabilities, and thus this suggested that very small changes in procedure, or in initial conditions, can profoundly affect the outcome of the experiment. These are characteristics of complex systems, but it has been unclear if they are confined to "artificial" systems (such as a beaker experiment on the ocean floor), or whether such instabilities could occur in a free release. We now have two additional examples of rapid, self-driven convective hydrate formation: one simply in liquid CO_2, and the other involving deep-sea sediments.

In a repeat of the experiment in Figure 2 (above) we did not observe simple dissolution of CO_2 into the aqueous phase. Instead we observed very rapid growth of hydrate lobes on the electrode cage that penetrated far into the liquid CO_2 phase (Figure 3).

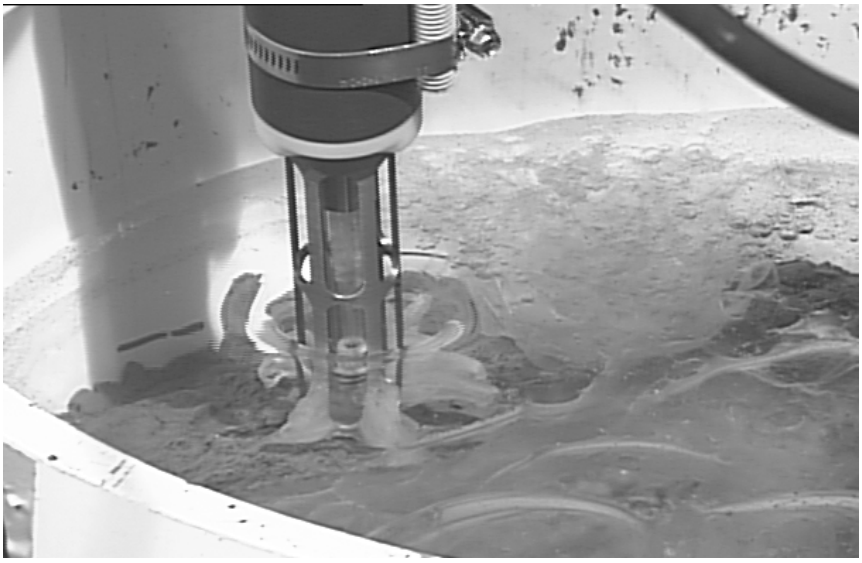

Figure 3: Image of pH electrode inserted into a pool of liquid CO_2. Hydrate nucleation has occurred, and rapidly growing lobes of hydrate extend several centimeters out into the CO_2 pool.

In Figure 4 we show an example of CO_2 penetration into sea-floor sediments, followed by formation of a "frost heave" from massive hydrate formation within the space of a few hours.

Figure 4: Formation of a massive "frost heave" of hydrate at 3600m in >>12 hours.

At present we can only give a descriptive account of this phenomenon which extends upon the account given by Aya et al. [10]. Sea water in contact with CO_2 forms a dense [11,12] saturated, or supersaturated, boundary layer with a thickness depending upon velocity in the bulk fluid. If the condition is quasi-diffusive this boundary layer may become thick enough to flow. If we now add a hydrate nucleation event then salt is rejected and heat released. For CO_2 the net effect is an increase in density, enhanced flow, and water from the bulk fluid is drawn in between the hydrate-CO_2 interface. This

leads to increased hydrate growth, and further fluid invasion in a self-propagating flow. Double diffusive properties may well come into play [13].

However we do not know what event triggers this condition. In the case of Figure 3 vibrations in the vehicle arm holding the electrode likely created the initial nucleation event. In Figure 4 no such trigger was present. While both liquid CO_2 and its hydrate dissolve in sea water the local changes (salt rejection, large volumetric changes etc.) created are quite different.

Conclusions and Future Research

The experimental science underlying study of possible deep-ocean CO_2 sequestration is advancing rapidly, and is greatly aided by ROV techniques which provide the experimental platform (manipulation, visualization, instrument support, data return). In this paper we focus on the physico-chemical properties of the system; the observations have large consequences for ideas of storage of a lake of CO_2 on the ocean floor, and are ripe for further investigation. For future work we have very recently developed and successfully deployed a laser Raman spectrometer [14] for *in situ* investigation of both hydrate formation [15], and detection of the fate of secondary chemical species. Companion studies on biological responses are also actively proceeding.

Acknowledgements

We acknowledge the support of the David and Lucile Packard Foundation, and of the U.S. Dept. of Energy Carbon Sequestration Program. This work would not be possible without the skilled support of the ROV Tiburon pilots, and the RV Western Flyer crew.

References

1. Brewer, P.G., Friederich, G., Peltzer, E.T. and Orr, F.M. Jr. (1999) *Science* **284**, 943.
2. Aya, I., Yamane, K., Kojima, R., Yamamoto, T. and Nariai, H. (2001) *Proc. 11th Intnl. Conf. Offshore & Polar Eng. Conf.*, Stavanger, Norway.
3. Brewer, P.G., Peltzer, E.T., Friederich, G. and Rehder, G. (2002) *Environ. Sci. Technol.* Submitted.
4. Orr, J.C. et al. (2001) *Greenhouse Gas Control Technologies GHGT-5*, Elsevier Science.
5. Aya, I., Yamane, K. and Nariai, H. (1997) *Energy* **22**, 263.
6. Mori, Y.H., and Mochizuki, T. (1998) *Energy Convers. Mgmt.* **39**, 567.
7. Broecker, W.S. and Peng, T.-H. (1982) In: *Tracers in the Sea*, Eldigio Press, pp. 113-130.
8. Santschi, P.H., Anderson, R.T., Fleisher, M.Q. and Bowles, W. (1991) *J. Geophys. Res.* **96**, 10,641.
9. Rehder, G., Brewer, P.G., Peltzer, E.T. and Friederich, G. (2002) *Geophys. Res. Lett.* In press.
10. Aya, I., Yamane, K. and Kojima, R. (2001) In: *Greenhouse Gas Control Technologies GHGT-5*, CSIRO, pp. 423-428.
11. Haugan, P. and Drange, H. (1992) *Nature* **357**, 318.
12. Ohsumi, T. (1993) *Energy Convers. Mgmt.* **34**, 1059.
13. Turner, J.S. (1995) In: *Geophys. Monograph 94*, Am. Geophys. Union, pp. 11-29.
14. Brewer, P.G., et al. (2002) *Eos, Trans. Am. Geophys. Union,* submitted.
15. Sum, A.K., Burrus, R.C. and Sloan, E.D. (1997) *J. Phys. Chem.* **101**, 7371.

ABSTRACT II
Copy of Manuscript on Deep-Sea Biological Responses

Title: Biological consequences of deep-sea CO_2 sequestration.

Authors: James P. Barry, Brad A. Seibel, Jeffrey C. Drazen, Mario N. Tamburri, Kurt R. Buck, Chris Lovera, Linda Kuhnz, Edward T. Peltzer, Karen Osborn, Patrick J. Whaling, Peter G. Brewer

Monterey Bay Aquarium Research Institute, 7700 Sandholdt Road, Moss Landing, CA 95039 (all authors)

Abstract

Ocean carbon sequestration by direct CO_2 injection may one day alter the chemistry of the deep ocean, and test the resilience of deep-sea ecosystems. Potential biological impacts of CO_2 sequestration for deep-sea organisms were evaluated *in situ* off California recently using small-scale (<100 liter) releases of liquid CO_2. Animals (echinoderms, crustaceans, and meiofaunal groups) exposed to low pH plumes resulting from dissolution of liquid CO_2 experienced high rates of mortality. Milder pH changes had few detectable effects. These results indicate that damage to deep-sea ecosystems from large-scale ocean carbon sequestration will depend on the volume and duration of CO_2 injection.

Direct injection of CO_2 into the deep-sea, a radical idea suggested 25 years ago (*1*), is now among several carbon management alternatives under serious consideration to offset the accelerating rise in anthropogenic greenhouse gas emissions (*2*). Globally, CO_2

emissions are expected to increase from present rates near 7 $GtCy^{-1}$ to 15 $GtCy^{-1}$ by 2050 (*3*). Although surface waters of the oceans absorb roughly 2 $GtCy^{-1}$ of anthropogenic CO_2 through air-sea gas exchange (*4*), this rate is insufficient to mitigate the rapid rise in atmospheric CO_2 and its expected climate impacts. Research is underway to investigate the chemistry and physics of CO_2 dissolution, sequestration efficacy under various injection scenarios, CO_2 separation and injection technology, and the environmental sensitivity of deep-sea ecosystems to perturbations in seawater chemistry caused by CO_2 injection. Although direct deep-sea CO_2 injection is technically feasible (*5*), the environmental consequences of large-scale CO_2 sequestration remain unknown and may be substantial.

Simulations of CO_2 injection at various locations and depths in the world ocean indicate that long-term (i.e. century-scale) sequestration is possible only if CO_2 is released into the deep-sea (ca. 3000 m) to prevent significant outgassing to the atmosphere over decadal scales (*6*). Because seawater is undersaturated with CO_2, injected liquid CO_2 or CO_2 hydrate will dissolve, producing a CO_2-rich, reduced-pH plume dispersed by deep-water currents. Dissolution and dilution near CO_2 injection sites will generate pH gradients from ~4.0 to background levels near 7.6 over spatial scales dependent upon the volume of CO_2 released, injection methods, and mixing rates. Assuming injection of 1 $gtC \cdot y^{-1}$, pH shifts of 1 unit will occur over 10s of km and more modest perturbations (0.1 – 0.3 pH shift) will develop over 100s to 1000s of km in the deep-ocean (*7*).

Although the biological consequences of direct ocean CO_2 injection for deep-sea ecosystems cannot yet be estimated, changes in seawater chemistry due to CO_2 addition will be stressful for a variety of deep-sea animals. Prolonged contact with liquid CO_2 is

almost certainly lethal for most animals and causes immediate death for the few species observed (*8*). Exposure to liquid CO_2 would only occur in the immediate vicinity of disposal sites, but CO_2 dissolution plumes may affect deep-sea ecosystems over large areas of the oceans.

Few studies have assessed the impacts of elevated CO_2 levels on deep-sea animals or microbial processes. Experiments on shallow-water organisms indicate a range of tolerance depending on ecotype, life stage, and phylogeny (*9*). Deep-sea animals, however, are expected to be far more sensitive than those inhabiting the upper ocean. Although the direct impacts of deep-sea CO_2 injection have not been reported, the deep-sea physiological literature suggests strongly that even small perturbations in seawater chemistry may be lethal for many deep-sea species (*10*).

Deep-sea CO_2 Release Experiments

We recently evaluated the effects of direct CO_2 injection on deep-sea animals *in situ* during two experiments involving small-scale releases of liquid CO_2 onto the seafloor off California. An ROV-mounted CO_2-release system developed by the Monterey Bay Aquarium Research Institute (MBARI) was used to inject liquid CO_2 into PVC corrals placed on the seafloor on the continental rise in 3600 m depth, 85 nm off Moss Landing, CA (36° 42’ 33.4” N, 123° 31’ 22.0”W). Liquid CO_2 is heavier than seawater at this depth and is contained within each corral, but dissolves slowly, producing a CO_2-rich, low-pH plume that drifts down-current. The effects of CO_2 plumes on the survival of various groups of deep-sea organisms were measured for several levels of plume exposure. Study organisms ranged from sediment-dwelling taxa (bacteria, meiofauna [<300 μm], and macrofauna [>300 μm]) that inhabit exposed

sediments, to epibenthic megafauna (urchins, holothurians) and near-bottom fishes that were held in cages exposed to CO_2 plumes.

In the first experiment (E1), 3 small (48 cm diameter x 15 cm high) PVC corrals were filled with twenty to twenty-five liters of liquid CO_2 (Fig. 1), and study animals were held in small (46 x 46 x 20 cm) mesh cages placed nearby (<1m). The survival of megafauna (urchins -*Cystechinus sp.*; holothurians - *Abyssocucumis sp*) held in cages and organisms inhabiting sediments adjacent to CO_2 corrals was compared with control groups near three empty corrals (*11*). A tube-building ampeliscid amphipod (*Haploops lodo*), the dominant infaunal taxon at the site, was collected in sediment cores along with other macrofauna, meiofauna, and bacteria before and after both experiments.

A second experiment (E2) was similar, but used a single, larger (93 cm diameter x 30 cm high) corral containing ~75 l of liquid CO_2. Study organisms included urchins and infaunal organisms used in E1, and common fishes (eelpout, *Pachycara sp.*; rattail, *Coryphaenoides armatus*). Fishes were collected in baited traps prior to CO_2 release, which were then closed to prevent additional capture. Fish traps and urchin cages were positioned 1, 5, 10, and 50 m from the central CO_2 pool. Infaunal organisms were sampled from sediment cores at these distances. CO_2 in experimental corrals dissolved continuously, but was replenished after ~2 weeks in each experiment to ensure continued CO_2 dissolution. Both experiments were terminated after ~1 month.

The intensity of plume exposure was estimated from pH sensors (*12*) located 1 m (E1), 5 m, and 50 m (E2) from CO_2 corrals. The direction and speed of near-bottom currents were measured using an acoustic doppler current meter (ADCP) during E1 (*13*).

Changes in Seawater Chemistry near CO_2 Pools

Dissolution of liquid CO_2 from corrals resulted in large peak pH perturbations (ΔpH ~ –1.5 units) within 1 m of the CO_2 corrals during E1 (Fig. 2). Excursions in pH greater than 1 unit were rare (<5% of the time), however, even near CO_2 pools, and reductions of –0.2 units or more occurred only 25% of the time. Due to instrument failure, no pH data are available for distances >1m during E1.

The CO_2 plume was generally weak 5 to 50 m from the CO_2 pool, where pH was measured during the second release experiment. Maximum pH shifts recorded 5 and 50 m from the CO_2 pool during E2 showed moderate (-0.2 pH units) to minor (-0.05) reductions, and small average changes (-0.008, -0.003 units), respectively. Shifts of -0.2 units were recorded less than 2% of the time 5 m from the CO_2 pool. Unfortunately, the pH sensor located 1 m from the central CO_2 corral failed during E2, but CO_2 dissolution appeared to be slower than observed during E1 (*14*). CO_2 initially filled the smaller corrals used in E1, and dissolved nearly completely in 2 weeks. In contrast, the higher-walled corral in E2 was initially ~1/3 full of CO_2, of which less than 50% dissolved after 2 weeks, perhaps related to hydrodynamics around the corral, the effects of sediment that settled on top of the CO_2, or both.

Due to the rotary character of inertial and tidal currents at the site, pH perturbations were episodic, exposing organisms to the CO_2 plume only during short periods when they were down-current of the CO_2 pool. Near-bottom currents during E1 averaged 4.4 $cm \cdot s^{-1}$, with net transport to the SE (118^o) at 1.7 $cm \cdot s^{-1}$ (Fig. 2). Fourier analysis of currents and variation in pH 1m (E1) and 5 m (E2) from CO_2 corrals all indicated strong periodicity near 12.4 h, associated with the major semidiurnal lunar tidal constituent (M2) that typically dominates tidal flow in this region. In effect, organisms

1m from CO_2 pools (E1) were bathed in pH-shifted waters of –1.0 or more units for about 30 minutes, twice per day (*15*). The CO_2 plume was an order of magnitude weaker 5 m from the CO_2 pool (E2) where pH shifts of ~0.1 unit or more persisted for ~15 minutes, twice per day.

Survival of Deep-Sea Organisms

The effects of exposure to CO_2 plumes on animal survival were severe near CO_2 pools where pH shifts were greatest. Few animals survived near CO_2 corrals during the first experiment, indicating the high vulnerability of a wide variety of animals to changes in seawater chemistry caused by CO_2-injection (Table 1). All urchins and holothurians near CO_2 corrals died during exposure and dissolution of skeletal elements was evident in several urchins (Fig. 3). Urchins in control cages appeared unharmed, and all holothurians in control cages were absent, and presumably escaped. Survival of the amphipod, *Haploops lodo*, was low after intense CO_2 exposure during E1. Its abundance and tissue condition (*16*) were initially similar among treatments, but differed greatly after one month, indicating mortality rates (% individuals moribund) of at least 95% near CO_2 pools, compared to only 7% near control corrals ($t=12.7$, $p<0.0001$). Sediment-dwelling meiofauna showed similar declines in population density or condition after exposure to intense CO_2 stress. The biovolume ($nl \cdot cm^{-2}$) of flagellates (0.83 vs. 0.75 $nl \cdot cm^{-2}$, $p<0.77$) and amoebae (0.93 vs. 1.12 $nl \cdot cm^{-2}$, $p<0.64$) were similar near CO_2 and control corrals before CO_2 injection, but their abundances near CO_2 pools declined during exposure (flagellates = 0.41, $p<0.005$; amoebae = 0.40; $p<0.026$), with little change near control corrals. The drop in the densities of both groups probably reflects the death and decay of individuals impacted by CO_2. Nematodes, the most prevalent meiofaunal group (71 % of the total meiofaunal biovolume), declined only slightly (5% reduction) in

biovolume near CO_2 pools, apparently due the slow degradation of their chitinous cuticle. Detailed inspection (*17*) of subsamples of individuals, however, indicated that most nematodes near CO_2 had died (~63%), compared to only ~16% near control stations ($p<0.005$). Unexpectedly, cell counts of sediment bacteria were similar between CO_2 and control corrals, despite the large pH shift and mortality of other groups, and even increased during the study near CO_2 (67.6 to 127.0 $x10^9$ cells·cm^{-3} and control (91.2 to 124.5 $x10^9$ cells·cm^{-3}) corrals. Several explanations for this pattern are possible, though no effect of CO_2 exposure is presently detectable.

Faunal responses to the apparently milder CO_2 plume produced during the second experiment were less severe than observed during E1, and decreased at distances of 5 m or greater where pH shifts were very small (Table 1). Although urchins held in cages within 1m of the central CO_2 pool died during E2, no obvious skeletal degradation was observed. Eight of ten urchins caged 5 m from CO_2 also died after exposure to pH reductions of only 0.1 to 0.3 units for less than 2% of E2 and an average pH shift of only –0.008. No CO_2 effects were observed for urchins held in more distant cages (10, 50 m) where pH changes were very small ($\Delta pH =< -0.05$ units less than 1% of E2). The mortality rate for amphipods (*Haploops lodo*) near (1m) the CO_2 pool was much lower during E2 (15%) than measured in E1 (95%), but was significantly ($p<0.04$) greater than initial values (Table 1). Reduced abundances of meiofaunal groups, observed during E1, was not detected from the few samples available near the CO_2 pool during E2.

The effects of CO_2 dissolution on deep-sea fishes were only tested during the second experiment and were inconclusive. All deep-sea eelpouts (n=5) survived near (1m, n=2; 5m, n=2) and distant (50 m, n=1) from the central CO_2 corral, despite their position on the bottom of cages (determined from time-lapse video) where the CO_2 plume

was most concentrated. In contrast, 3 rattails (*C. armatus*) caged 1 m from the CO_2 pool died, as did 3 individuals each held in cages 5 and 50 m from CO_2.

Patterns of mortality observed in this study indicate the vulnerability of several deep-sea marine taxa to shifts in pH caused by CO_2 injection, and support the expectation (*10*) that deep-sea species may be particularly intolerant of pH stress that will accompany a direct CO_2 injection sequestration program. Shallow water animals, by contrast, are more tolerant of pH shifts. Mortality rates for various shallow-water animals exposed continuously (rather than intermittently) in laboratory studies to pH changes of –1 unit or greater for days to weeks (*9*) were lower than observed in this study.

Although our experiments produced the changes in seawater chemistry expected under a large-scale CO_2 injection program, their small scale and intermittent plume exposure due to shifts in current direction complicates interpretation of lethal pH levels. Were high mortalities observed during the first experiment caused by exposure to brief (~1 $h \cdot d^{-1}$), but intense (ΔpH ~1 unit or more) CO_2 plumes or by the impacts of moderate (ΔpH ~0.1 units) but more persistent (~6-8 $h \cdot d^{-1}$) plume exposure? Animal mortality was much lower distant (5m) from CO_2 pools, but was, nevertheless, detectable for urchins and infaunal amphipods over the month-long experiments even after very brief (30 $min \cdot d^{-1}$) exposure to pH shifts of only –0.1 units and average pH changes of -0.008 units. Future studies will include refined methods to evaluate the response of typical midwater and benthic deep-sea animals and microorganisms to relatively constant CO_2 plume intensities.

Survival of fishes exposed to CO_2 plumes during E2 remains unexplained and requires further study. Although the respiratory proteins of *C. armatus* are extremely sensitive to pH (*18*), the death of rattails near and distant from CO_2 is very likely a result

of caging during the experiment and cannot be attributed to CO_2 exposure. *C. armatus* has also died in studies not involving CO_2 (*19*) after being held in cages for several days. Survival of all eelpouts is surprising, considering that 4 individuals were 1 to 5 m from the CO_2 pool. It is unclear whether these fishes are tolerant of pH stress or if they were able to reduce activity during brief periods of exposure to the CO_2 plume, then recover when currents carried the plume away from cages. Tissue analyses and additional studies are planned to evaluate CO_2 effects on important deep-sea fishes, as well as a broad spectrum of midwater and benthic organisms.

Mechanisms of pH stress

Immersion in CO_2-laden, acidic seawater from CO_2 injection poses physiological challenges to marine animals that will respond by tolerance, compensation, or death, based on physiological repertoires that have evolved over thousands of generations. Deep-sea animals have evolved in highly stable, food-poor conditions typical of deep-ocean waters and, in general, are much more sensitive to a variety of environmental perturbations than shallow-water animals, including those associated with CO_2 injection (10).

CO_2 readily crosses biological membranes (e.g. gills) leading to acidosis in the intra- and extracellular fluids. The general mechanisms used by organisms to combat acidosis are similar whether the perturbation is environmental (i.e. CO_2 sequestration) or endogenous (metabolic or respiratory). Species that undergo high levels of activity are adapted for control of exercise-based tissue acidosis, and may be pre-adapted for tolerance of environmental hypercapnia (elevated CO_2). In contrast with the exercise – rest behavior of animals that allows for pH compensation, chronic immersion in

hypercapnic waters may overwhelm the acid/base regulation potential of many marine animals. Less active animals, as is typical of most deep-sea species, may be even less tolerant of pH changes.

Extracellular (blood) acidosis reduces the oxygen affinity of most respiratory proteins, including those of deep-sea species (*10*), thereby reducing the aerobic scope of activity for these animals. Intracellular acidosis may result in metabolic depression (torpor), limiting activity, growth, and reproductive output (*20*). *In situ* experiments (*21*) documented narcosis in Pacific hagfish (*Eptatretus stoutii*), a deep-sea fish that exhibited little to no aversion to CO_2 – enriched seawater. Preliminary information (*22*) on the survival of other deep-sea fishes suggests that CO_2 and pH have different effects.

Physiological stress associated with chronic exposure to CO_2 injection plumes, if not lethal, will almost certainly convey higher "costs of living" through the energetic costs of acid / base balance, restricted aerobic capacity, and inhibition of protein synthesis. These costs may be particularly high for deep-sea organisms, which may have limited metabolic scope (*10*) due to their sedentary life styles in the food-poor waters of the deep-sea. Physiological impacts of CO_2 exposure for individuals will translate to changes in the survival, growth, and reproduction rates of populations, and shifts in the ecosystem dynamics of deep-sea communities.

Ecosystem risks for direct ocean CO_2 sequestration

The scale of ecosystem impacts to be expected from direct CO_2 sequestration depends on the depth, location, and certainly the volume of CO_2 injected. Since any CO_2 released will result in CO_2 dissolution plumes from pH ~ 4 to background values, animals in the vicinity of disposal sites are at great risk. Plume effects over larger scale may be

estimated coarsely from expected pH fields. For example, if 0.25 to 4 $gtCy^{-1}$ as CO_2 is injected for 100 y beneath 3000 m and disperses worldwide, the pH of the deep-waters of the entire world ocean will shift by –0.02 to –0.3 units (*23*, greater than the mean and maximum ph shifts 5m from our CO_2 pools). More severe shifts in pH will occur in mixing zones that may extend 10s to 100s of km around disposal sites. Results from this study and the deep-sea physiological literature indicate that an aggressive ocean CO_2 sequestration program (i.e. near 4 $gtC{\cdot}y^{-1}$) will cause substantial damage to deep-sea ecosystems. Even a moderate sequestration effort, however, may impact the survival of individuals, populations, and species, for a wide variety of deep-sea organisms.

Our initial investigations of the sensitivities of deep-sea marine organisms to CO_2 injection provide only a glimpse of the possible effects of anthropogenic perturbations to deep-sea chemistry that will occur on a global scale if a direct ocean CO_2 sequestration program is implemented. Much additional research on the biological impacts for deep-sea organisms, including benthic and midwater taxa spanning all important phyla, as well CO_2 effects on microbial processes, is required before reasonable estimates of the ecosystem consequences of a sequestration program are possible.

Direct deep-sea CO_2 sequestration could partially mitigate the anthropogenic rise in atmospheric pCO_2 that will almost certainly accelerate through this century. CO_2 "injection" into the surface ocean by way of air-sea exchange of waste CO_2 emitted to the atmosphere has already decreased the pH of surface waters by 0.1 units. Concern for the effects of continued acidification and warming on various shallow marine ecosystems or populations including coral reefs (*24*, *25*), salmon fisheries (*26*), polar marine ecosystems (*27*, *28*) has prompted research to evaluate the effects of unchecked increases in atmospheric CO_2. Given the low probability that sufficient progress will be made toward

reduction of fossil fuel consumption, the decision to implement a direct ocean CO_2 sequestration program hinges on the balance between the lesser of two evils – the unabated effects of climate warming on terrestrial and shallow marine ecosystems or damage to deep-sea ecosystems by CO_2 sequestration. Ongoing research should provide guidance concerning the risks of direct CO_2 injection, and may mandate other methods or more environmentally benign CO_2 sequestration approaches such as accelerated carbonate dissolution (*29*). Clearly, an ocean carbon sequestration program will be successful only if its intended benefits – a stabilization of atmospheric CO_2 and mitigation of climate warming consequences for terrestrial and shallow water ocean systems, outweigh its liabilities – energy expended on sequestration and damage to deep-sea ecosystems. Lacking presently is sufficient information on both sides of this balance.

References and Notes

1 C. Marchetti, *Climate Change* **1**, 59 (1977)

2 U.S. Dept. of Energy, Carbon Sequestration: Research and Development (1999; www.ornl.gov/carbon_sequestration/)

3 G. Marland, T.A. Boden, R.J. Andres, Global, Regional, and National CO_2 Emissions. In Trends: A Compendium of Data on Global Change. Carbon Dioxide Information Analysis Center, Oak Ridge National Laboratory, U.S. Department of Energy (2001; http://cdiac.esd.ornl.gov/trends/trends.htm)

4 J.T. Houghton et al., Climate Change: The IPCC Scientific assessment. Intergovernmental Panel on Climate Change, Cambridge University Press (1990)

5 IEA Greenhouse Gas R&D Programme, Ocean Storage of CO_2 , ISBN 1 898373 25 6, (1997)

6 J.C. Orr et al., *Eos Trans. AGU*, **81** (48), Fall Meet. Suppl., Abstract B11D-09, (2000)

7 K. Caldeira, M.E. Wickett, *Eos. Trans. AGU*, **83**, Ocean Sciences Meet. Suppl., Abstract OS51F-01 (2002)

8 In association with deep-sea CO_2 release experiments, we exposed a variety of deep-sea species to direct contact with liquid CO_2. All individuals (1 to 3 individuals each) of holothuroids (Peniogone sp., Scotoplanes sp.) and ophiuroids (unknown sp.) died within seconds of direct contact.

9 D.I. Auerbach, J.A. Caulfield, E.E. Adams, and H.J. Herzog, *Env. Modeling and Assessment*, **2**, 333 (1997)

10 B.A. Seibel, P.J. Walsh, *Science*, **295**, 275 (2001)

11 Five individuals each of urchins (Cystechinus sp.) and holothurians (Abyssocucumis sp.) were collected from the seafloor nearby using a suction sampler and placed carefully in each mesh cage adjacent to CO_2 corrals (n=3) and control corrals (n=3). Sediment cores (7.5 cm diameter x 20 cm deep) were collected to obtain mud samples for microbial, meiofaunal, and macrofaunal counts and analyses (n=6 per corral). Sets of sediment cores were collected prior to dispensing the CO_2 and after 35d exposure. Macrofaunal samples were sieved (300 μm). Meiofaunal analyses based on percol-gradient centrifugation technique. Microbial counts performed under epifluorescence microscopic inspection of DAPI-stained samples. Abundance, biovolume, or indices of mortality (e.g. tissue degradation) were compared among treatments at the beginning and end of the experiment.

12 pH measurements were made using combination CTD/pH sensors positioned ~3-5 cm above the seafloor during both experiments. Time-series records of pH were obtained from 1 m away from a CO_2 pool during E1 (pH data series = 9.4 d), and from 5 m

(24.7 d series), and 50 m (27 d series) from the central CO_2 corral during E2. Several additional CTD/pH sensors failed during the experiments, preventing comparisons of pH plumes between experiments.

13 An ACDP was deployed 2 m above the bottom during E1. Currents 15 m above the bottom (bin 1) were used for analyses. Current records were not obtained during E2.

14 CO_2 corrals used in E1 were 15 cm high, and filled completely with liquid CO_2, leading to fairly rapid dissolution, likely due to the direct exposure of the CO_2 surface to near bottom currents. During E2, a single larger PVC corral (33 cm high x 94 cm diameter) was filled only 2/3 full, partially insulating the CO_2 surface from bottom currents. This appears to have resulted in a slower dissolution rate and perhaps smaller pH excursions around the corral.

15 The intensity (magnitude of pH reduction) and duration of CO_2 plume exposure events were analyzed from each pH time series. Because of the rotary to oscillatory currents with ~semidiurnal periodicity (12.4 h), CO_2 plumes drifted in the same direction roughly twice per day. Rates of dissolution declined during two-week periods after CO_2 pools were filled, resulting in progressively milder shifts in pH with time. Thus, the duration of a particular magnitude of pH reduction depended on the time since CO_2 pools were filled.

16 Because animals collected from 3600 m depths die upon ascent to the surface, mortality caused by CO_2 exposure must be distinguished from death during ascent. We assessed the degradation state of amphipod tissues using a rating system from 1 (intact, “recent death”) to 5 (nearly entirely degraded, tissues translucent to transparent, exoskeleton fragile). Ratings of 4 or greater had certainly been dead for at least 2 weeks, based on comparisons with tissue degradation rates of amphipods

measured at the site in separate assays. Thus, mortality (percent of individuals dead) was calculated as the percentage of all individuals with tissue ratings of 4 or higher.

17 Subsamples of nematodes were inspected under epifluorescence microscopy after staining with DAPI, which illuminates cell nuclei. Lack of intact cell nuclei indicates that the animals had died at least several days prior to collection.

18 R.W. Noble et al., *Biochimica et Biophysica Acta*, **870**, 552 (1986)

19 D. Bailey and M. Priede, personal communication

20 H-O. Portner, A. Reipschlager, Pages 57-81 in Ocean Storage of CO_2. Environmental, IEA Green house and Gas R & D Programme, (1996)

21 M.N. Tamburri *et al*., *Marine Chemistry*, **72**, 95 (2000)

22 J. Kita, T. Kikkawa, A. Ishimatsu, A. 2000. Tokyo Inst. of Technology, Proc. 2nd Int. Sym. on Ocean Sequestration of Carbon Dioxide and Joint Int. Con. on CO_2 Fixation and Efficient Utilization of Energy, 93 (2000).

23 Estimates of pH changes in the deep-sea caused by 100 y of CO_2 sequestration using injection rates of 0.25 and 4 gtCy-1 were calculated assuming no outgassing of injected CO_2 from the volume of the bottom 1 km of the ocean (~3.6 x 108 km-3), alkalinity = 2400 μm.kg-1, depth = 3500 m, T = 1.5 C, initial ΣCO_2 = 2350 μm.kg-1, and ending ΣCO_2 = 2356 and 2443 μm.kg-1, respectively.

24 J.A. Kleypas *et al*., *Science*, **284**, 118 (1999)

25 N. Knowlton, *PNAS*, **98**, 5419 (2001)

26 D.W. Welch, Y. Ishida, K., Nagasawa, Can. J. Fish. & Aquat. Sci. 55, 937 (1998).

27 I. Stirling, *J. Mar. Systems* **10**, 9 (1995)

28 R.C. Smith *et al*., *Bioscience* **49**, 393 (1999)

29 K. Caldeira, G.H. Rau, *Geophys. Res. Let*. **27**, 225 (2000)

This research was supported by MBARI (projects 200001, 200002), the U.S. Dept. of Energy, Fossil Energy Group (Grant DE-FC26-00NT40929), and the U.S. Department of Energy, Ocean Carbon Sequestration Program, Biological and Environmental Research (BER), (grant #DE-FG03-01ER63065). Deep-sea experiments would not have been possible without the excellent support of the crews of the R/V Western Flyer and ROV Tiburon.

Table 1. Summary of faunal impacts during CO_2 release experiments. pH shifts in heading rows are the maximum and (mean) perturbations to ambient pH levels during each experiment. Cell values are percentage mortality estimates based on comparisons of CO_2 vs. Control treatments (E1) or initial vs. end samples (E2). CO_2 impacts were high for samples within areas of large pH shifts, and undetectable or non-significant for small pH shifts. Negative mortality listed for bacteria indicates an increase in cell counts. Failure of pH sensors prevented measurements of pH shifts near (1m) the CO_2 pool during E2. All faunal groups except bacteria exhibited high rates of mortality near CO_2 pools in E1. E1, E2 indicated Experiment 1, and 2, respectively. Blanks indicate no data. ns, *, **, *** indicate non-significant, $p<0.05$, $p<0.01$, $p<0.001$ for t-tests.

Summary of CO_2 Impacts	**1 m (E1)**	**1 m (E2)**	**5 m (E2)**	**10 m (E2)**	**50 m (E2)**
Change in pH units: Max (mean)	-1.0 (-0.2)	?	-0.1 (-0.008)	?	-0.01 (-0.003)
Bacteria	-2.0 ns				
Meiofauna					
Flagellates	64.1 **				
Amoebae	66.9 *				
Nematodes	63.0 **	0	0		
Macrofauna					
Amphipod *Haploops lodo*	95.3 ***	14.8 *	1.9 ns	3.2 ns	2.9 ns
Epibenthic Megafauna					
Urchin - *Cystechinus* sp.	100.0 **	100	80	0	0
Holothurian - *Abyssocucumis* sp	100.0 **				
Near-Bottom Deep-Sea Fishes					
Zoarcid – *Pachychara sp.*		0	0		0
Macrourid - *Coryphaenoides armatus*		100	100		100

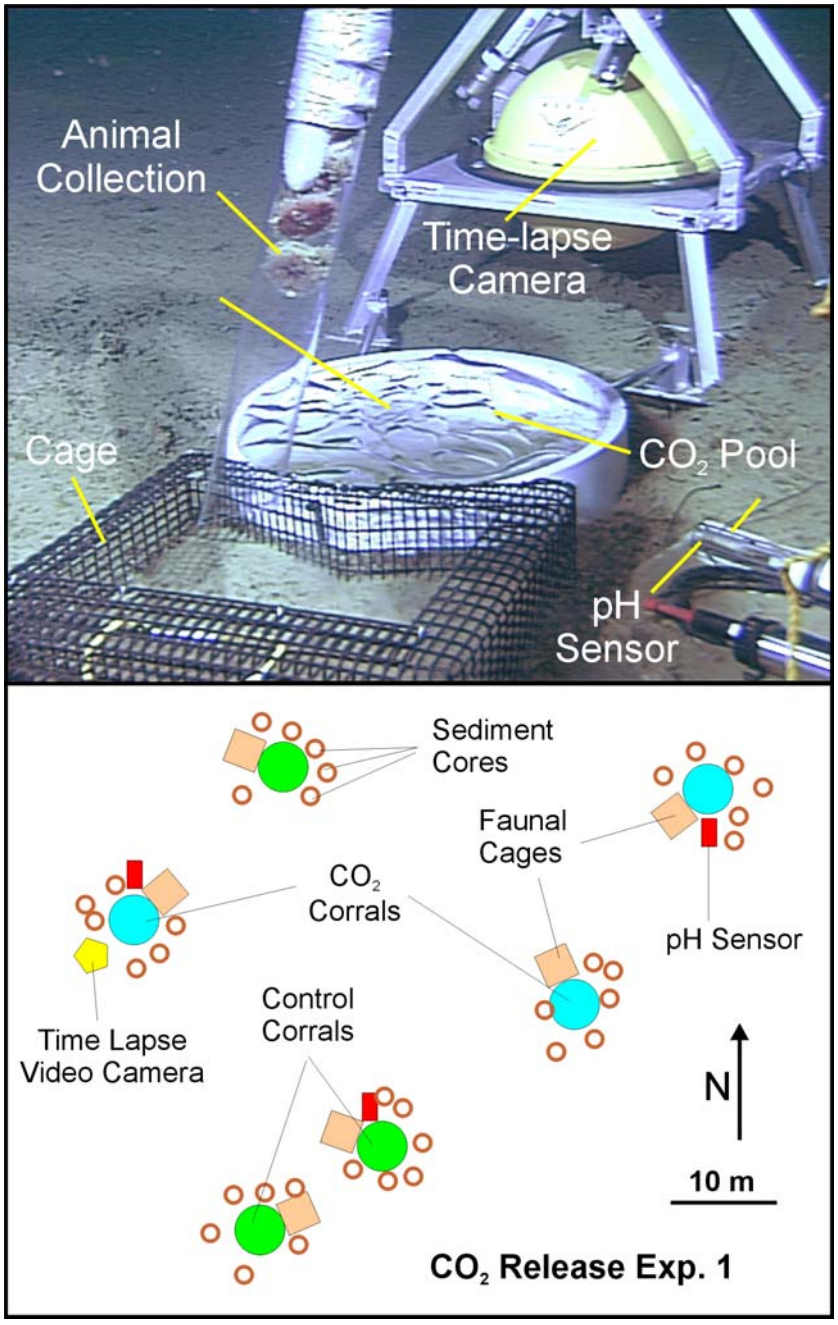

Figure 1. CO_2 Release Experiment 1. CO_2 corral filled with liquid CO_2, animal cage used to hold megafauna, pH sensor, and time-lapse video camera used in E1 (top). Sea urchins and holothurians are visible in acrylic tube, used as suction sampler to collect and deploy megafauna. Experimental layout of CO_2 release E1 at 3600 m depth shown in bottom image.

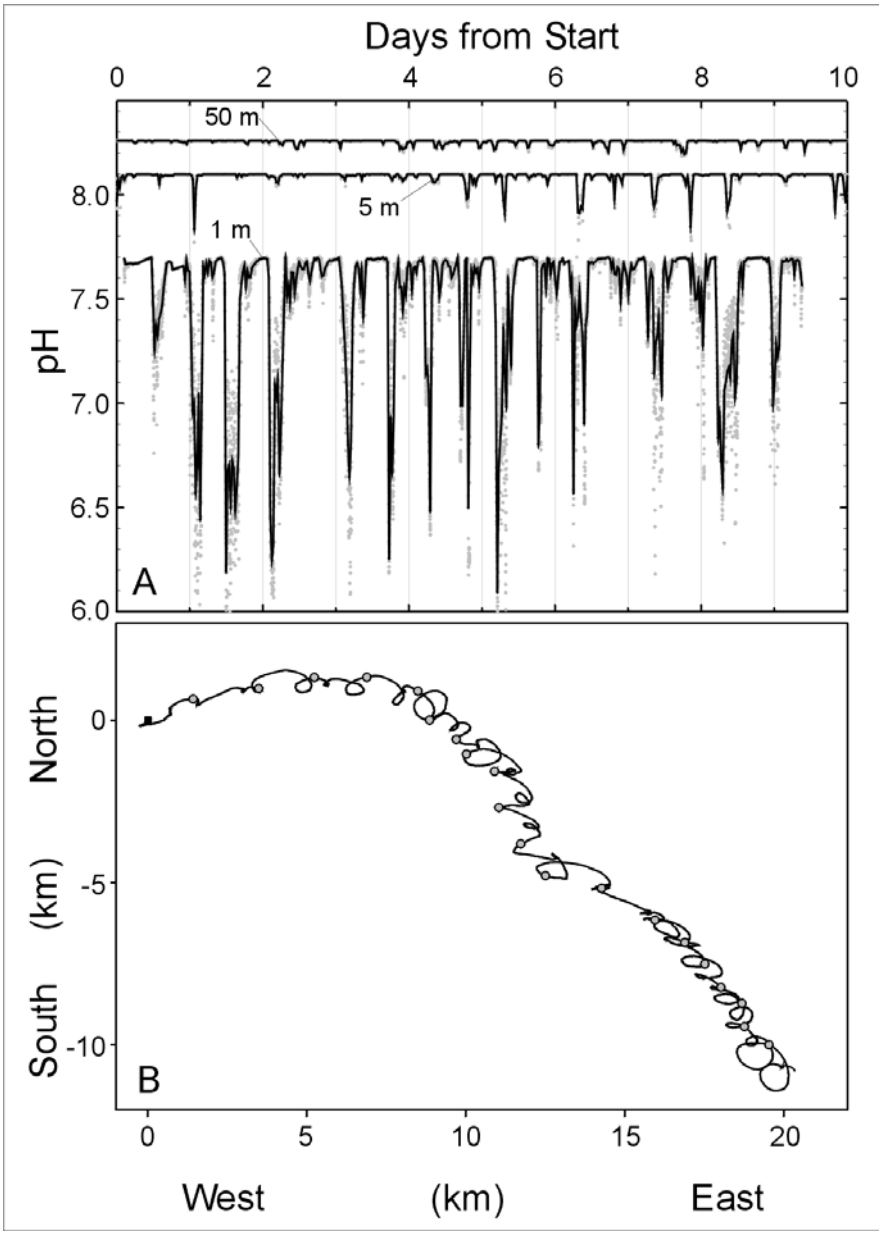

Figure 2. a. pH records from CO_2 releases E1 (1 m data) and E2 (5, 50 m data). 5 m data are offset by +0.5 units. 50 m data offset by +0.75 pH units. B. Progressive vector diagram of current flow at the experiment site during E1, showing rotary inertial and tidal currents with general drift to the SE. Starting point indicted by black box, start of each day indicated by gray circles.

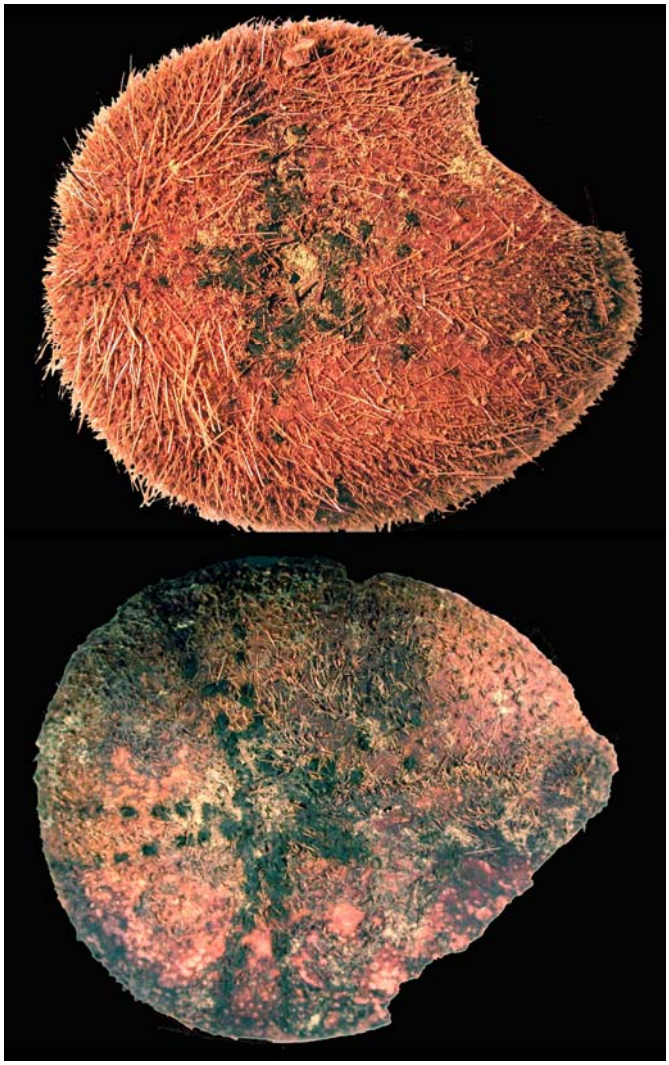

Figure 3. Dissolution of urchin skeletal elements from exposure to CO_2 plumes during E1 is evident in light micrographs of air-dried urchin tests (length ~6 cm). Urchin test at bottom shows dissolution at base after 30 d exposure to intermitent pH changes of >1.0 units. Upper image shows normal condition of base of urchin test from control corral.

APPENDIX III

Copy of Paper on CO_2 Droplets Submitted to Environmental Science & Technology

Experimental Determination of the Fate of a CO_2 Plume in Sea Water

Peter G. Brewer,[*1] Edward T. Peltzer[1], Gernot Friederich[1], and Gregor Rehder [1,2]
[1]Monterey Bay Aquarium Research Institute, 7700 Sandholdt Road, Moss Landing CA, 95039, USA
[2] Present address: GEOMAR, Center for Marine Research, Wischhofstr. 1-3, D-24148, Kiel, Germany
* Corresponding author telephone: 831-775-1706; fax: 831-775-1620; e-mail: brpe@mbari.org

---

Abstract

Direct oceanic disposal of fossil fuel CO_2 is being considered (*1,2)* as a possible means to moderate the growth rate of CO_2 in the atmosphere. We have measured the rise rate and dissolution rate of freely released CO_2 droplets in the open ocean to provide fundamental data for carbon sequestration options. A small amount of liquid CO_2 was released at 800m depth and 4.4°C, and the rising droplet stream was imaged with a HDTV camera carried on a remotely operated vehicle. The initial rise rate for 0.9-cm diameter droplets was 10 cm/sec at 800m, and the dissolution rate was 3.0 μmol/cm^2/sec. While visual contact was maintained for 1 hour and over 400m, 90% of the mass loss occurred within 30 minutes and 200m above the release point. Images of droplets crossing the liquid-gas phase boundary showed formation of a gas head, pinching off of a liquid tail, and rapid separation and dissolution.

Introduction

The disposal of fossil fuel CO_2 in the deep ocean has long been discussed as a means of ameliorating greenhouse gas induced climate change (*3,4*). Although models of this

process have been formulated (*5,6*), and laboratory simulations have been carried out (*7-9*), there have been few direct oceanic experiments reported. With the availability of advanced Remotely Operated Vehicle (ROV) technology it has now become possible to carry out controlled releases of many chemical species in the deep sea, and to observe and measure the processes taking place. In earlier work (*10*) we have reported on the contained mid-water release of both CH_4 and CO_2 to form hydrates. Here we report on the more difficult problem of observing and accurately measuring the behavior of a rising stream of freely released CO_2 in order to evaluate the behavior and dissolution rate of droplets in dynamic motion in the open ocean.

An accurate description of the fate of CO_2 injected into ocean water is necessary for proceeding with any ocean disposal procedure. At shallow depths (above about 350m, depending upon the local temperature gradient) CO_2 is a gas, and will readily dissolve. Below this depth we encounter the gas hydrate phase boundary, again dependent on local conditions, and a shell of CO_2-hydrate may be generated (*11,12*) which can have profound consequences; and below about 400m depth the gas-liquid transition occurs. Each of these regimes can have distinct reaction rates and characteristics. The low compressibility of sea water, and the high compressibility of liquid CO_2, results in a density ratio reversal at high pressure such that below about 3000m depth a gravitationally stable release can be achieved (*13*) under typical ocean conditions. Release at depth leads to long oceanic residence times and effective sequestration from the atmosphere (*14*). Yet the potential cost and technical difficulty of deep injection

suggests the need for evaluating injection at shallower depths (*6*), which in certain ocean areas may be very effective.

Laboratory studies have been very successful in identifying both the CO_2 hydrate phase boundary, and the characteristics of the solid phase (*15*). But it is difficult for a laboratory study to simulate correctly the behavior of freely released material in motion with changing bubble dynamics and surface film characteristics, and thus models have necessarily been created and differing conclusions reached. Holder et al. (*16*) modeled the behavior of a rising CO_2 plume in the case of a constantly growing film of solid hydrate. Since CO_2-hydrate is more dense than either seawater or liquid CO_2 itself then this would slow the rise rate, and eventually cause sinking. Herzog et al. (*5*) modeled the dissolution rate of liquid CO_2 with no hydrate film released at depths between 500 and 2000m. They concluded that if the initial drop radius is less than 1 cm, then complete dissolution would occur within less than 200m. A very complete set of model calculations incorporating plume dynamics has been carried out (*6,17*), and yet no field data exist to compare these models against.

Experimental

Our experiments took place at 800m depth in Monterey Bay, California. The depth was chosen to match plans for an international experiment designed primarily to study plume dynamics of CO_2 released in the deep ocean (*18*).

Remotely Operated Vehicle. We used the ROV *Ventana* (*10*), deployed by the RV *Point Lobos* for our work. The viewing system on Ventana used for real-time observation and permanently recording visual images utilizes the digital "high-definition" television format. The system captures images with a specially modified Sony HDC-750 high-definition television camera which digitizes the picture data and formats it to the SMPTE 292M HDTV interface standard with 2:1 interlace. The resolution of the images is 1080 pixels vertically and 1920 pixels horizontally which is about five times the resolution of conventional video. The image data is continually uplinked from the ROV to the ship for display and simultaneously recorded with a Panasonic HD2000 high-definition video tape recorder without any further transcoding steps. Still frame grabs obtained from the 30 frames/sec recording were captured (Viewgraphics Corp.), and processed using standard image processing software (Photoshop®).

CO_2 Release and Imaging. Early work had shown that it was impossible to obtain accurate size data, and maintain within the field of view a CO_2 droplet cloud that was free to move in all dimensions. Lack of a dimensional reference, effects of the vehicle motions, strong lateral forcing due to local currents, and the similarity of appearance of a droplet of liquid CO_2 to the ubiquitous gelatinous marine organisms, all combined to frustrate continuous observation. Therefore we constructed a simple imaging box (Figure 1), 89 cm long, 25 cm deep, and with a transparent face 30 cm wide, open to the ocean at top and bottom, and mounted this directly in the camera field of view. The purpose was to restrain lateral motions, while permitting free upward motion of the droplet plume. The opaque back of the box rejected visual clutter from marine snow in the far field. A meter

scale was fixed to the box and was maintained within the imaged field at all times. The injection technique was modified slightly from that described earlier (*10*), and used a piston assembly, operated by the vehicle hydraulic system, with a displacement capacity of 500ml. The CO_2 was delivered to the ocean through a 1/8-inch orifice mounted on the back of the imaging box.

While the concept of this experiment is disarmingly simple, the execution is hard. It requires the precise piloting of a 3 ton vehicle, subject to oceanic forcing in 3 dimensions, while imaging a small cloud of droplets with millimeter precision for one hour over hundreds of meters of ascent. It is a tribute to the skill of the pilots that this was achieved.

Results

CO_2 in the liquid phase. Three experiments were carried out. In the first release the droplet was contained for 21 minutes, rising from 800m to 625m depth, at which time the droplet escaped from the imaging space. In a second release a droplet was followed from 800m to 340m depth over a period of about 1 hour: the depth versus time curve of the ascent was recorded by the conductivity-temperature-depth (CTD) sensor attached to the vehicle. In Figure 2 we show the temperature profile recorded during the experiments, overlaid on the phase diagram for CO_2 in seawater.

Several droplet release experiments were carried out. For one release a mean ascent rate of 12.8 cm/sec was obtained. For another, longer, experiment the mean rise rate was 12.4 cm/sec. However, for this experiment the data indicate a measurable increase in velocity

with decreasing pressure and diminishing size; the initial rise rate was 10.2 cm/sec, increasing gradually to 14.9 cm/sec at depths shallower than 450m (Table 1).

The simple picture of a single purely spherical droplet proved unrealistic. It was soon observed that bubble collision was frequent, and we observed rafts of CO_2 droplets that would remain strongly attached to each other for very long periods. It is not known whether a large-scale field release would show such droplet associations. For our work it was necessary to recognize a distinctively shaped unit for following within the droplet cloud. We found such a unit, which formed a droplet pair as shown in Figure 3. The changing dimensions of these droplets during their ascent are given in Table 1. These complex shapes, rotating in three dimensions as they move, presented varying aspect ratios to the camera and frame grabs were carefully selected to remove this effect.

Droplet collision with, and sticking to, the walls of the box did occasionally occur. It was possible to free the droplet with a lateral ROV thruster kick, but because of the possibility of mass loss to the walls, rather than by dissolution, these data were eliminated. The walls of the box inevitably created boundary flow conditions as the vehicle rose, and droplets were consistently drawn to this boundary flow region. In spite of these difficulties it proved possible to maintain the droplets in free flow for the ascent, thus any bias due to boundary effects is likely small. This is supported by the smooth rise observed (Figure 4a).

The imaging box was of known dimensions, and a meter scale was attached to the rear wall of the box and always in view. We thus have numerical reference points with which to quantify the images of droplets during ascent. The time at which an image was recorded was logged on the same time base as the vehicle depth (pressure), temperature etc. Frame grabs from the HDTV video tape were taken at times (shown by the circles in Figure 4a) when the bubble aspect ratio presented to the camera was consistent with long axis view, and droplet dimensions measured with a software cursor compared to the numerical scale. Parallax corrections for the distance between the front and rear walls of the imaging box were made to compensate for differences in imaging the rear mounted scale, and the tendency of droplets to migrate to the front of the box, as observed by a second, downward looking, camera.

Also in Table 1 we give the data recorded on droplet size versus depth, and we calculate the mass loss with time. These results show that the droplet diameter changes as a linear function of time, and give a dissolution rate for liquid CO_2 of 3.0 μmol/cm^2/sec (Figure 4b). We may compare this result, from a rising plume traversing a 8 – 4 MPa pressure gradient, with the results of Aya et al. (*7*) from laboratory pressure vessel studies at 30 MPa and 4.5°C; the laboratory measurements yield a value of 2.8 μmol/cm^2/sec. The agreement is excellent given the lower pressures and the higher temperatures involved, and the complex fluid dynamics of a rising droplet stream (*18*).

The liquid-gas transition. In these first releases we looked for a change in rise rate coincident with the transition from droplet to bubble on crossing the liquid-gas phase

boundary, but could not observe this, probably due to the very small droplet size at that point. The data can be smoothly fit with a second order polynomial with no evidence of a discontinuity at that point, although data above this phase boundary are limited. As the droplets rise they shrink from dissolution, expand from pressure release, and encounter progressively warmer and less dense sea water. The net result of this complex process is the small increase in rise rate that we observe.

We carried out another release in a specific attempt to observe processes occurring at the gas-liquid transition. From Figure 2 we find that this should occur at about 400m, and droplets were released just below that point and observed as before. In Figure 5 we show an image of this transition: this illustrates the processes at work. The droplet first becomes opaque, possibly due to the formation of nascent gaseous, hydrate covered, CO_2 on the warming outer surface, and a clear "head" of the emergent gas forms, pushing through the hydrate shell. The buoyant effect of the gas head stretches the remnant liquid droplet, creating a neck, which pinches off creating an accelerating bubble and a lagging droplet. Note that in this oceanic region both gas and liquid phases are within the hydrate phase boundary. In other regions (Mediterranean Sea, Sargasso Sea) warmer deep water depresses the hydrate phase boundary and differing processes may occur.

Presence of a hydrate film. In earlier work (*10,13*) we have demonstrated that within the appropriate phase boundary CO_2 clathrate hydrate forms readily, almost instantaneously, on vigorous mixing of CO_2 and sea water. Gas hydrate formation is often recognizable by a change in optical reflectivity of the surface, and by a white cloudy appearance.

However when formed by liquid-liquid contact a pure, transparent, solid is formed. Evidence here of the stiffness of the liquid droplet surface, and its spherical shape, formed immediately after injection, clearly indicate the presence of a hydrate skin. Conditions in the delivery tube promoted hydrate formation, and droplet rafts formed and maintained a stick like shape immediately after release; as the droplets rose they became more rounded. Other work in our laboratory strongly supports the hydrate skin phenomenon. We have carried out similar studies of the fate of a hydrate-forming methane plume in sea water, and compared this directly with argon as a comparative, non-hydrate forming, gas (*19*). The results showed that the presence of a hydrate film reduced CH_4 dissolution rates by a factor of 4, and this is supported for CO_2 by laboratory studies of dissolution rates (*7*). Holder et al. calculate a reduction in dissolution rate of a factor of 3 for CO_2 released at 1000m depth (*20*).

The standard model for both gas (*21*) and solid (*22*) dissolution rates in the ocean invokes saturated boundary theory, and we may expect this also to apply to liquid-hydrate-liquid interactions. For velocities of 8 cm/sec diffusive boundary layers of about 500μm are reported (*22*), and we estimate boundary layer dimensions close to 300μm for the 12 cm/sec rise rates observed in our experiments. Thus the rates observed here at relatively shallow ocean depths may be extended by calculating saturation values in equilibrium with the hydrate at different P,T values. Laboratory saturation data are available (*7*), and values may also be readily calculated (Multiflash, Infochem Ltd.); from these results we find that dissolution rates at depth should be no more than a factor of 2 slower than those reported here.

Modeling the rising behavior of liquid CO_2 droplets. Now that we have measured the dissolution rate of liquid CO_2 under upper ocean conditions and rising at an appropriate velocity, we can construct a simple numerical model of the released CO_2 droplet based upon the buoyancy of a rigid sphere. This model is iterative and contains no arbitrarily adjustable parameters. We release a droplet of pre-determined size at some depth and temperature, then follow it upwards in a stepwise calculation. Acceleration is assumed to be instantaneous, and the upwards velocity is determined by the spherical buoyancy equation:

$$U = [8 \bullet g \bullet r \bullet (\rho_{sw} - \rho_{CO2} / (3 \bullet \rho_{CO2})]^{0.5}$$

where U is the terminal rise velocity for a rigid sphere, g is the acceleration of gravity, r is the droplet/sphere radius and ρ_{sw} and ρ_{CO2} are the changing in situ densities of seawater and liquid CO_2, respectively.

After a suitably short time interval chosen to give high resolution and precision, we calculate the droplet's new position (depth) and determine its density based upon the ambient pressure (computed for this depth (*23*)) and temperature (obtained from the local temperature gradient) at this point. For this first approximation of a droplet rise model, we interpolated the density of liquid CO_2 from tabulated values for pure CO_2 at 0ºC and 10ºC (*24*). The remaining mass is calculated based upon the measured dissolution rate (above) and the droplet size. The new droplet size is then determined from the remaining

mass and computed density, and a new upwards velocity is computed. This process is repeated until the droplet reaches 500 m at which point liquid CO_2 at 10ºC becomes a gas and it is no longer possible to interpolate the density of liquid CO_2 at the in situ temperature and pressures.

The results of this model are shown in Figure 6. We begin by choosing the release depth and droplet size as observed in our experiment. Our objective is to numerically simulate or predict the droplet behavior. In Figure 6a we see that the predicted depth / rise rate of the liquid CO_2 droplet, exactly matches the observed release. Likewise, in Figure 6b, we see that the predicted droplet size and mass fraction remaining are also a good match to the experimentally obtained data. Thus we conclude that this simple model is a fairly accurate predictor of the behavior of liquid CO_2 droplets in the deep sea. It is also interesting to note that while this model is based solely upon the behavior of pure CO_2, it is likely that in the oceanic environment that the CO_2 droplet was rapidly equilibrated with seawater and quickly became saturated with water. Any effect that the saturation of liquid CO_2 with water had on either the rise rate or the dissolution rate was obviously small. Indeed, in Table 2, we see that the calculated solubility of water in liquid CO_2 at the relevant temperatures and pressures is vanishingly small and has little impact on the density so the choice of pure CO_2 as the modeled substance was reasonable.

Discussion

Ocean disposal of CO_2 is but one sequestration option, and within the oceanic realm the choice of water column dissolution from a rising stream of CO_2, or the formation of a

sinking plume with hydrate formation (*13*) as a large-scale ocean CO_2 disposal option has yet to be made. The results obtained here should allow a more accurate prediction of the CO_2/pH field, and the environmental effects, surrounding an injection point.

So far we have considered the droplet plume as having the properties of pure CO_2. However additional components are very possible, for example absorption of water, and non-polar species, into the CO_2, and surface adsorption of material. Surface adsorption onto bubbles is well known in the gas transfer literature as the "dirty bubble" problem (*25*). However we saw no evidence of this affecting droplet behavior even though our experiments took place in a biologically rich environment.

A critical property for the longer term will be the effectiveness of this form of sequestration. For example the depths chosen here cover the 27.3 – 26.8 (σ_θ) isopycnal surfaces. The 26.8 surface is the most dense seawater to outcrop seasonally at the surface in the North Pacific, and the ventilation age of this surface has been mapped by Warner et al. (*26*). This probably represents the shallowest depth at which disposal in this ocean basin is likely to be effective. The strong density increase created in CO_2 saturated seawater at relatively shallow depths can lead to sinking plumes, and such disposal scenarios have been elegantly considered (*27*) for North Atlantic sites.

The small-scale ROV experiments described here appear to offer an effective way to evaluate these processes, without the cost and environmental permit requirements for large-scale releases. We are not able with these small quantities to easily simulate some

of the changes in local seawater density, and "peeling" of the plume due to large-scale fluid dynamic effects (*18*). It is possible to extend these small scale studies to include biological effects (*28*), and this work is in progress.

Acknowledgements

We thank the pilots of the ROV Ventana for their exceptional skills. This work was supported by a grant to MBARI from the David and Lucile Packard Foundation, and by the U.S. Dept. of Energy Ocean Carbon Sequestration Research Program Grant # De-FC26-00NT40929.

Literature Cited

(1) U.S. Dept. of Energy. *Carbon Sequestration Research and Development*, Oak Ridge National Lab., **1999**.
(2) Brewer, P.G. *Oceanography* **2000**, *13*, 84.
(3) Marchetti, C. *Climate Change* **1977**, *1*, 59.
(4) N. Handa and T. Ohsumi, *Direct Ocean Disposal of Carbon Dioxide* **1995** (Terra Scientific Publishing, Tokyo, pp 274).
(5) Herzog, H., Golomb, D., Zemba, S. *Envir. Prog.* **10**, 64 (1991).
(6) Drange, H., Alendal, G., Johannessen, O.M. *Geophys. Res. Lett.* **2001**, *28*, 2637.
(7) Aya, I., Yamane, K., Nariai, H. *Energy* **1997**, *22*, 263.
(8) Hirai, S., Okasabi, K., Tabe, Y., hijikata, K., Mori, Y. *Energy* **1997**, *22*, 285.
(9) Shindo, Y., Hakuta, T., Fujioka, Y., Koiyama, H. *Energy Convers. Mgmt.* **1995**, *36*, 479.
(10) Brewer, P.G., Orr, F.M. Jr., Friederich, G., Kvenvolden, K.A., Orange, D.L. *Energy & Fuels* **1998**, *12,*183.
(11) Sloan, E.D. Jr., *Clathrate Hydrates of Natural Gases, 2nd edition* **1998** (Dekker, New York).
(12) North, W.J., Blackwell, V.R., Morgan, J.J. *Environ. Sci. Technol.* **1998**, *32*, 676.
(13) Brewer, P.G., Friederich, G., Peltzer, E.T., Orr, F.M. Jr., *Science* **1999,** *284*, 943.
(14) Orr, J.C. et al. *Greenhouse Gas Control Technologies* 2000, *2*, Elsevier Science
(15) Sum, A.K., Burruss, R.C., E.D. Sloan, Jr. *J. Phys. Chem. B* **1997,** *101*, 7371.
(16) Holder, G.D., Cugini, A.V., Warzinski, R.P. *Environ. Sci. Technol.* **1995,** *28*, 276.
(17) Alendal, G., Drange, H. *J. Geophys. Res.*, **2001**, *106*, 1085.
(18) Adams, E., et al. In: G*reenhouse Gas Control Technologies* **1999**, Elsevier, 293.
(19) Rehder, G., Brewer, P.G., Peltzer, E.T., Friederich, G. *Geophys. Res. Lett.* **2002**, In press.

(20) Holder, G.D., Warzinski, R.P. *Prepr. Pap. Am. Chem. Soc. Div. Fuel Chem.* **1996**, *41(4*), 1452.
(21) Broecker, W.S. and Peng, T.-H. *Tracers in the Sea* **1982** (Eldigio Press).
(22) Santschi, P.H., Anderson, R.T., Fleisher, M.Q., Bowles, W. *J. Geophys. Res.* **1991**, *96*, 10,641.
(23) Millero, F.J., Poisson, A. *Deep-Sea Research* **1981**, *28A,* 625.
(24) Perry, J.H., ed. *Chemical Engineers' Handbook, 3rd Ed.* **1950** (McGraw-Hill, New York) p. 206.
(25) Clift, R., Grace, J.R., Weber, M.E. *Bubbles, Drops and Particles* **1978** (Academic Press, New York).
(26) Warner, M.J., Bullister, J.L., Wisegarver, D.P., Gammon, R.H., Weiss, R.F. *J. Geophys. Res.* **1996** *101,* 20,525
(27) Haugan, P., Drange, H. *Nature* **1992**, *357*, 318.
(28) Tamburri, M.N., Peltzer, E.T., Friederich, G.E., Aya, I., Yamane, K., Brewer, P.G. *Mar. Chem.* **2000**, *72*, 95.

Table 1

Measured Liquid CO_2 Droplet Characteristics during Ascent from 800m Depth

Elapsed Time (min)	Depth (m)	Temp. (°C)	Droplet Diameter (cm)		CO_2 Density (g/cc)	Amount of CO_2 (millimoles)		Rise Rate (cm/s)
			(a)	(b)		(a)	(b)	
0	804.5	4.398	0.890		0.9423	7.89		10.2
14.23	706.3	4.740	0.606		0.9310	2.47		11.3
23.13	649.1	4.994	0.485	0.890	0.9235	1.25	7.74	12.0
29.82	602.1	5.165	0.364	0.728	0.9171	0.52	4.21	12.5
43.08	496.8	5.449	0.162	0.647	0.9021	0.05	2.91	13.5
49.73	447.3	5.995		0.364	0.8910		0.51	14.0
61.65	341.2	7.291		0.202	0.8632		0.08	14.9

The initial droplet tracked (a) was joined at about 650 m depth by a second, larger, bubble (b) which became attached. No change in rise rate could be detected due to the attachment, and the changing size of each droplet could be independently determined. The mean density of liquid CO_2 during the rise of the droplets was 0.92 (a) and 0.90 (b), respectively. Thus, a 1 cm^3 droplet contains 21.1 (a) or 20.4 (b) millimoles CO_2. We calculate the dissolution rate (Γ) from the slope of:

$$(r_t - r_0) \;=\; -\,V_m \times \Gamma \times (t - t_0), \qquad [1]$$

where V_m is the specific volume (cm^3/mmol), r_0 and r_t are initial droplet radius and droplet radius at time t, and t_0 and t are initial time and the time elapsed since t_0. The observed dissolution rate was 3.0 μmol/cm^2/sec.

Table 2

Calculated H_2O Solubility in Liquid CO_2 and Density of Liquid CO_2

Depth	Hyd P	Abs P	Temp	% H_2O	Density of CO_2 Pure	Density of CO_2 + H_2O
m	dbar	MPa	deg C	mole	g/cm^3	g/cm^3
400	403.5	4.136	6.42	0.0021	0.89251	0.89254
500	504.5	5.146	5.44	0.0019	0.90992	0.90995
600	605.5	6.157	5.18	0.0017	0.92051	0.92053
700	706.6	7.167	4.76	0.0016	0.93086	0.93088
800	807.7	8.179	4.41	0.0015	0.93992	0.93993

The solubility of water in liquid CO_2 and the density of liquid CO_2 was calculated for five depths and the appropriate ambient temperature conditions using Multiflash® software (Infochem Computer Services Ltd, London). Water solubility in liquid CO_2 at these conditions was calculated using the RKSA-infochem model which includes the formation of CO_2 clathrate hydrate as the solubility limiting condition. Subsequently, the liquid CO_2 density was calculated, either for the pure liquid or for the water saturated liquid CO_2 using the Multiflash® implementation of the LKP equation of state. As can be seen in the table, the density differences are very small, on the order of 0.00001-0.00003 g/cm^3, and are probably not significant within the capabilities of the model.

Figure Captions

Figure 1. Rear view of the imaging box mounted on a rigid frame in front of the ROV. The HDTV camera is at the right side of the picture. Gas and liquid CO_2 injection lines feed into the back of the box, and below these a pH electrode is mounted on the white block.

Figure 2. The observed ocean temperature profile recorded during the droplet rise experiments, overlaid on the CO_2 phase diagram for seawater at a salinity of 34. The injection point is far inside the region for hydrate formation, the droplet crossed the gas-liquid phase boundary at about 400m depth, and visual contact was lost at about 340m depth**.**

Figure 3. Image of the two CO_2 droplets tracked during ascent as they cross the scale (mm. divisions). The bubbles are in free motion with a mean upward velocity of 12 cm/sec. The image was taken from a video frame grab at 654m depth, 23 minutes after release. The droplets became attached and moved together, but did not merge and their dimensions could be separately determined.

Figure 4. (a) Vehicle depth versus time for the experiments reported here. Pressure and temperature are recorded continuously on the vehicle and converted to depth using the seawater equation of state and local gravity. Circles represent locations at which frame grabs were taken for image analysis yielding the data in Table 1. **(b)** Plot of the changing droplet diameter with time, and remaining mass fraction of the droplets. The droplet size derived from HDTV video analysis, as listed in Table 1, is shown by circles (droplet-a) and pluses (droplet-b), respectively. The dashed line indicates the least squares fit of equation 1(Table 1); the slope gives a dissolution rate of 3.0 $\mu mol/cm^2/sec$. The solid line shows the remaining mass fraction relative to the initial mass of the CO_2 droplets.

Figure 5. CO_2 droplet evolution in crossing the liquid-gas phase boundary, while still within the hydrate stability zone. This shows formation of a gas head, which stretches the droplet to form a waist, which then pinches off as the emergent gas bubble accelerates.

Figure 6. Results of the rising droplet model calculations plotted against the observed behavior of liquid CO2. **(a)** Position of the rising droplet (dashed line) versus the actual ROV depth (circles) at 2.5 minute intervals. **(b)** Modeled droplet diameter (dashed line) and modeled mass fraction remaining (dot-dash line) versus the data for droplet-a (circles and squares) and droplet-b (pluses and crosses), respectively.

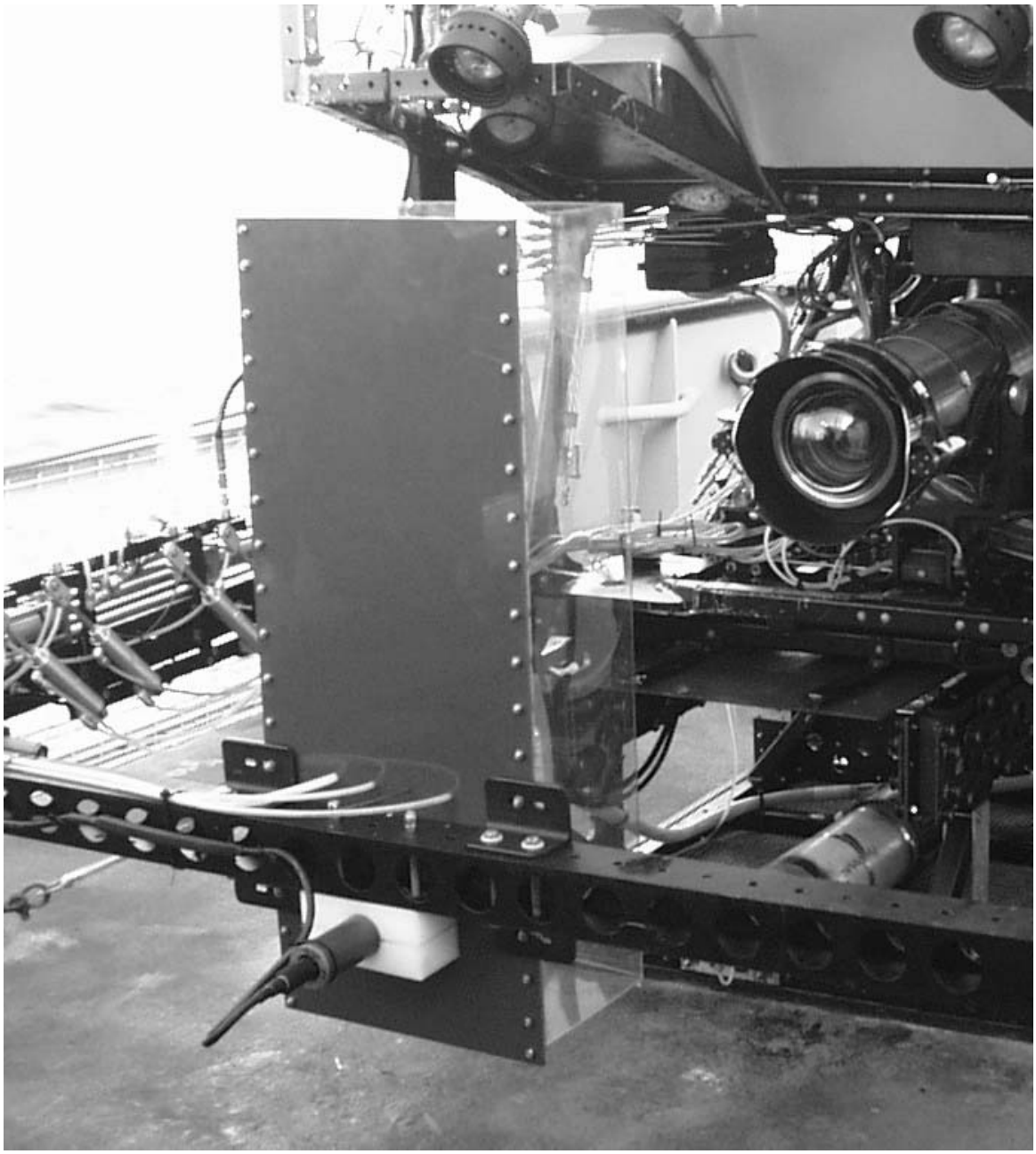

Figure 1

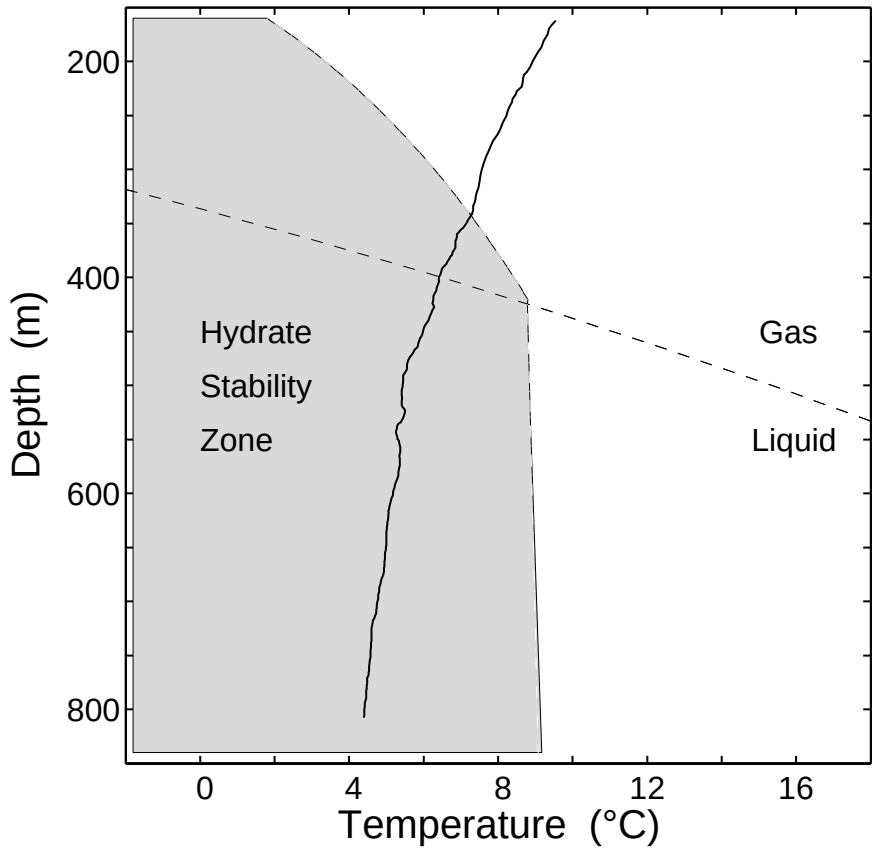
200
400
600
800
Depth (m)
Hydrate
Stability
Zone
Gas
Liquid
0
4
8
12
16
Temperature (°C)

Figure 2

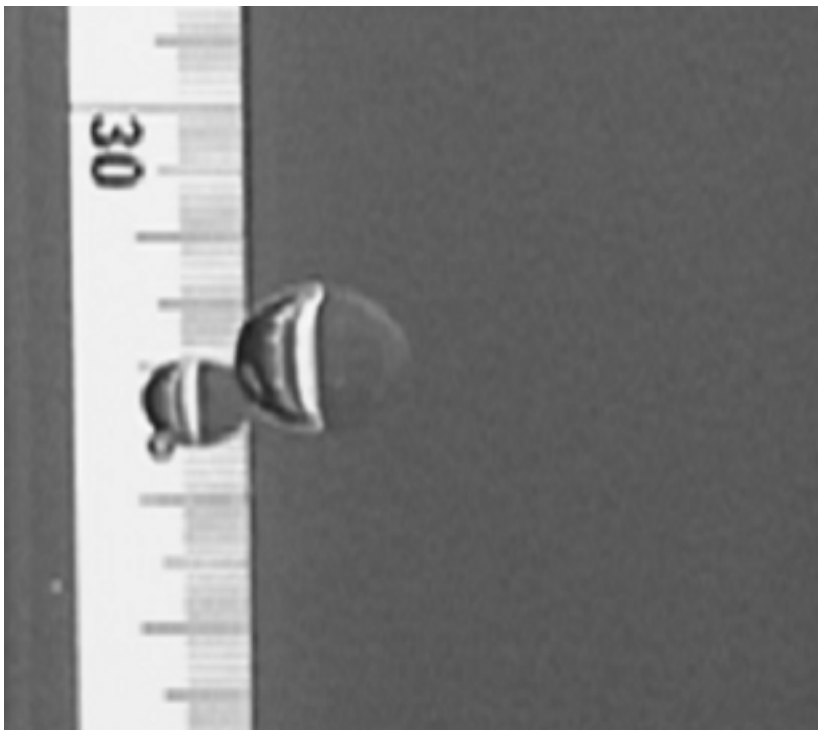

Figure 3

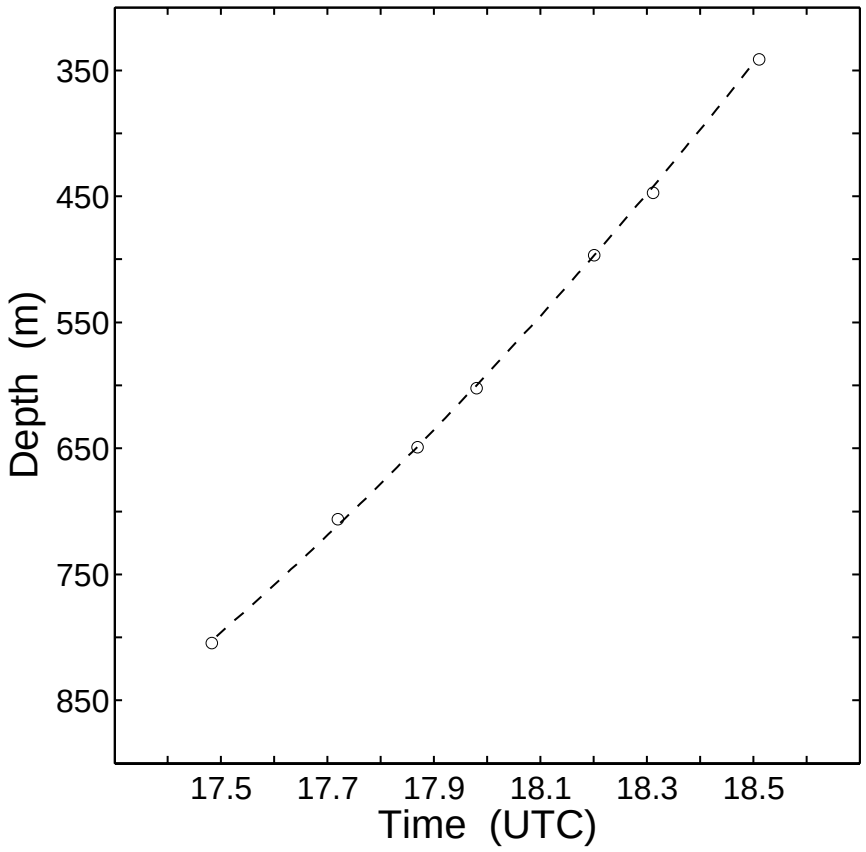

Figure 4a

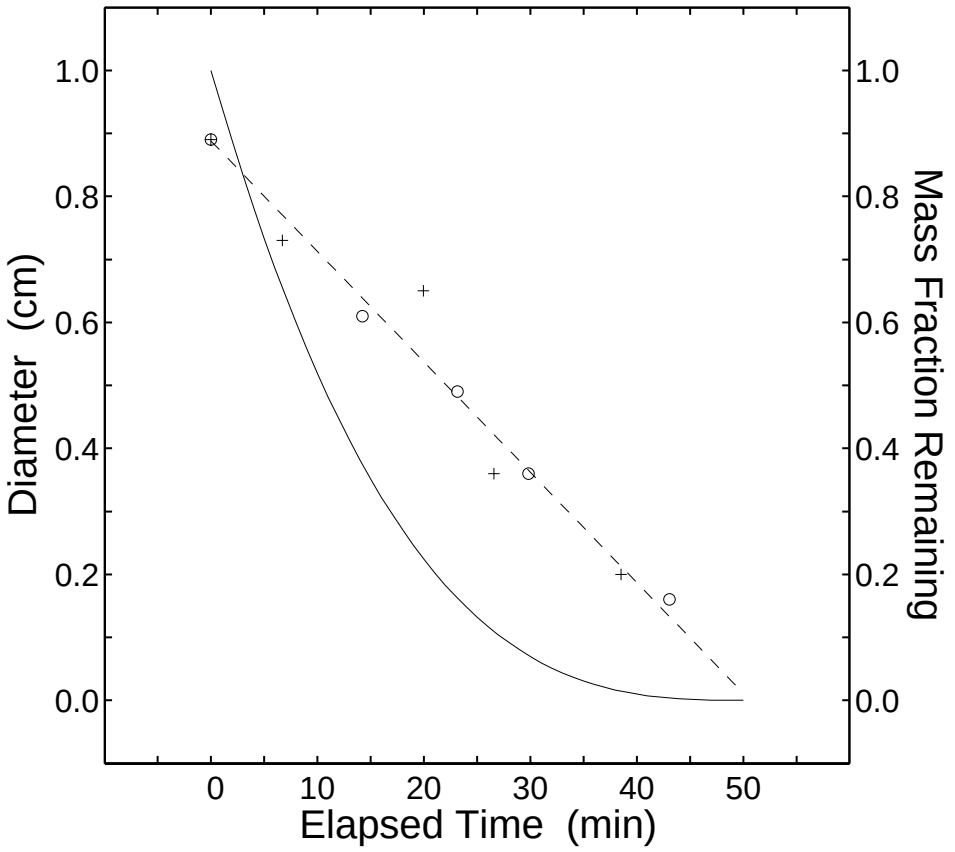
Diameter (cm)
Mass Fraction Remaining
Elapsed Time (min)
0.0
0.2
0.4
0.6
0.8
1.0
0
10
20
30
40
50

Figure 4b

Figure 5

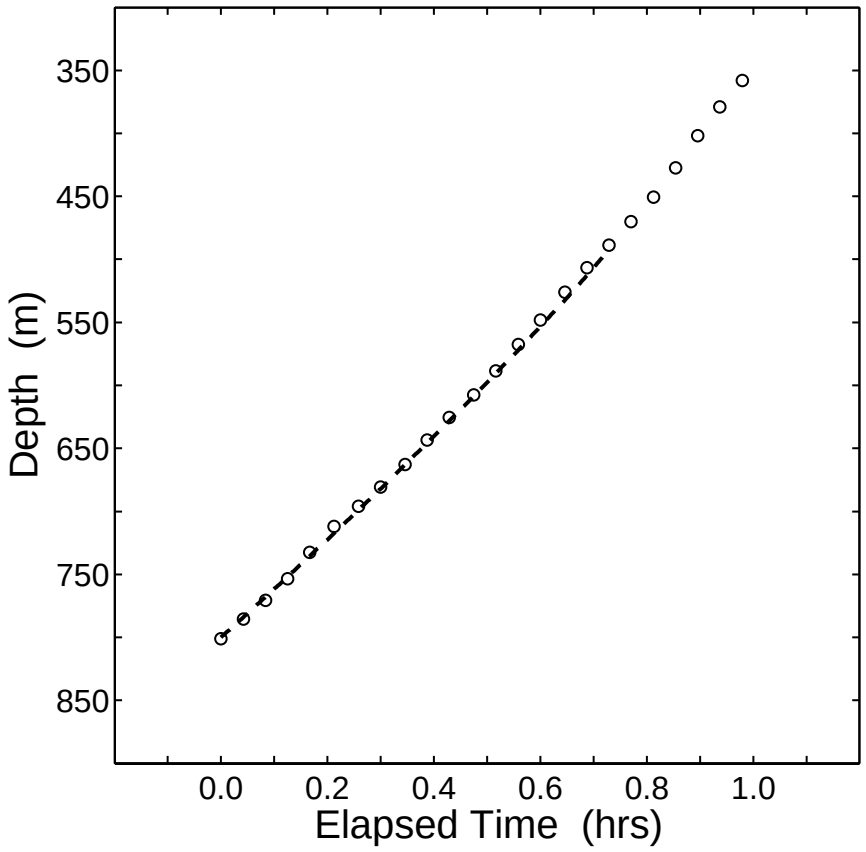
350
450
550
650
750
850
Depth (m)
0.0
0.2
0.4
0.6
0.8
1.0
Elapsed Time (hrs)

Figure 6a

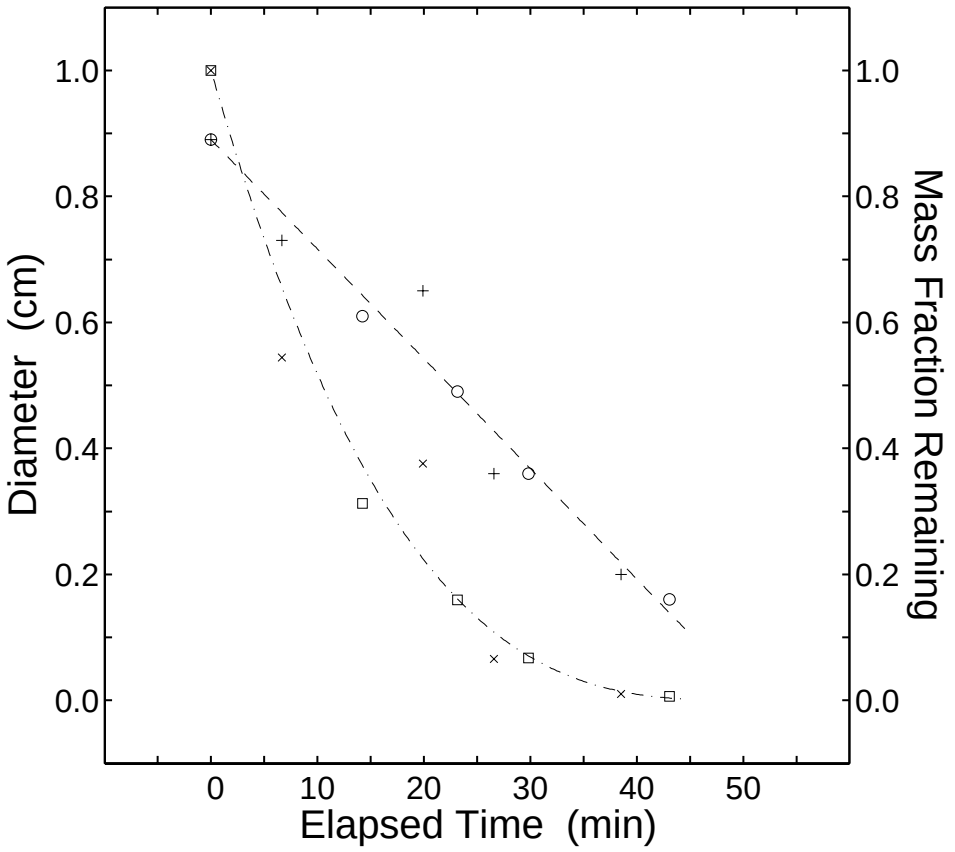
Diameter (cm)
Mass Fraction Remaining
Elapsed Time (min)
0.0
0.2
0.4
0.6
0.8
1.0
0
10
20
30
40
50

Figure 6b

APPENDIX IV

Copy of Article on Laser Raman Spectrometry of Deep Ocean CO_2 In Press in Eos

Laser Raman Spectroscopy at 3600m Ocean Depth

Peter G. Brewer, Jill Pasteris, George Malby, Edward Peltzer, Sheri White, John Freeman, Brigitte Wopenka, Mark Brown, Danelle Cline.

For additional information contact Peter Brewer, Monterey Bay Aquarium Research Institute, Moss Landing CA 95039, USA; E-mail: brpe@mbari.org

Making geochemical measurements in the deep ocean is fundamentally difficult. For this reason, century-old technologies using water bottles and cores for sample recovery still provide the basic tools. With the development of research submersibles and remotely operated vehicles (ROVs), however, new opportunities for sophisticated sampling and analysis have arisen. We report here on the first deployment of a laser Raman spectrometer for *in situ* deep-ocean science. Raman spectroscopy has its origins in ocean science, for it was the "wonderful blue opalescence of the Mediterranean Sea" that first stimulated C.V. Raman to investigate the molecular scattering of light [*Raman,* 1930]. Many laboratory results of laser-excited Raman spectroscopy are applicable to deep-ocean research. The identification and characterization of minerals, the speciation of dissolved complexes and gases, chemical-structural characterization of gas hydrates [*Sum et al.,* 1997], and sulfur speciation in filamentous benthic bacteria [*Pasteris et al.*, 2001] provide important examples. The latter two represent especially important ocean geochemical targets that are best studied *in situ*.

The instrument we adapted is a Kaiser Optical Systems HoloProbe® spectrometer with a HoloPlex® transmissive holographic grating and an Andor CCD array detector. The

exciting laser is a 532-nm, frequency-doubled Nd:YAG laser yielding ~30 mW at the probe head. The instrument was housed in three pressure cases for ocean deployment: one held the laser and a single-board computer, a second the spectrometer and CCD detector, and the third held the optical probe head (see Fig. 1) that both projected the laser beam and captured the back-scattered Raman radiation.

The system was accommodated on the ROV Tiburon [*Brewer et al.*, 1999] and deployed on four successful dives to a maximum of 3610m depth. The spectrometer and laser housings remained on the ROV tool sled, while the probe head (connected by fiber-optic cable) was manipulated by the robotic arm to bring the laser into focus on the sample (Fig. 1b). The instrument was controlled from the surface ship using the Kaiser HoloGRAMS® software over an ethernet link through the vehicle fiber-optic tether. Wavelength-calibration of the spectrometer was done in the laboratory with a neon-emission lamp and on deck and at depth using isopropanol and diamond as standards. The calibration protocols are being refined to quantify depth-related effects on the spectrometer due to both temperature change and pressure-induced deformation of the housing. For measurements made at depth, the accuracy in reported peak position currently is ± 3 cm^{-1}, whereas the precision is ± 0.4 cm^{-1}.

We obtained Raman spectra of sea water throughout the water column to characterize both instrument performance and the ocean background medium, and also *in situ* spectra of several-centimeter calcite cleavage fragments that were transported to depth. We are using the instrument to investigate oceanic sequestration of fossil fuel CO_2 [*Brewer et al.,*

1999]. Spectra were taken of CO_2 injected *in situ* into an inverted glass beaker at 200m depth and changes observed during transit to 664m. Results show the band shifts associated with changes in the density of CO_2, including the spectrally obvious gas-liquid phase transformation. Liquid CO_2 was also injected at 3600 m depth either directly onto the sea floor (spectrum in Fig. 1a), into a glass beaker (Fig. 1b), or into specially designed corrals. The growth of CO_2 clathrate hydrate, the formation of secondary solid and dissolved species, the formation of CO_2-saturated boundary layers, and the dissolution of sea floor minerals due to introduction of CO_2 are future targets of Raman investigation.

Hydrothermal vents on the sea floor and their associated bacterial mats are other ideal future candidates to take advantage of Raman spectroscopy's ability to characterize solids, liquids, and gases. Both CH_4 and H_2S vent gases are excellent Raman scatterers. Raman spectra provide information on molecular-structural speciation, which can permit the distinction between polymorphs (e.g., calcite vs. aragonite, wurtzite vs. sphalerite), as well as inferences about oxidation state (e.g., SO_4^{2-} vs. H_2S) and pH (e.g., SO_4^{2-} vs. HSO_4^-) in deep ocean environments.

Acknowledgements
We thank the pilots of the ROV Tiburon, and the crew of the RV Western Flyer. We acknowledge support of the David and Lucile Packard Foundation, and the U.S. Dept. of Energy Ocean Carbon Sequestration Program.

References

Brewer, P.G., G. Friederich, E.T. Peltzer, and F.M. Orr, Jr. Direct experiments on the ocean disposal of fossil fuel CO_2, *Science 284*, 943-945,1999.
J.D. Pasteris, J.J. Freeman, S.K. Goffredi, K.R. Buck, Raman spectroscopic and laser scanning confocal microscopic analysis of sulfur in living sulfur-precipitating marine bacteria, *Chem. Geol. 180*, 3-18, 2001.
Raman, C.V., The molecular scattering of light, *Nobel Lecture* (1930).
Sum, A.K., R.C. Burruss, and E. Dendy Sloan, Jr., Measurement of clathrate hydrates via Raman spectroscopy, *J. Phys. Chem. 101*, 7371-7377, 1997.

Figure 1. A) Raman spectrum of liquid CO_2 placed directly on sea floor sediments (image not shown). Spectrum shows two strong bands of the Fermi diad for CO_2, as well as the background spectrum of sea water, including the H_2O bend (~1630 Δcm^{-1}), O-H stretch (~3400 Δcm^{-1}), and S-O stretch (~984 Δcm^{-1}; bulk sea water SO_4^{2-} concentration is about 28 mM).

B) 532-nm laser beam exiting the Raman probe head (in its pressure housing) during spectral acquisition from liquid CO_2 in a 4-l beaker (15.5 cm in diameter) on the sea floor at 3607m depth, 1.5°C.